Electrochemical Carbon Dioxide Capture and Concentration

Alessandra M. Zito†[a], Lauren E. Clarke†[b], Jeffrey Barlow†[a], Daniel Bím†[c], Zisheng Zhang[c], Katelyn Ripley[b], Clarabella Lia[a], Amanda Kummeth[a], McLain E. Leonard[b], Anastassia N. Alexandrova*[c], Fikile Brushett*[b], Jenny Y. Yang*[a]

†equal contribution
[a] Department of Chemistry, University of California, Irvine, California 92697, USA
[b] Department of Chemical Engineering, Massachusetts Institute of Technology, Cambridge, MA, USA
[c] Department of Chemistry and Biochemistry, University of California, Los Angeles, Los Angeles, California 90095-1569, USA
*ana@chem.ucla.edu, Brushett@mit.edu, j.yang@uci.edu

Abstract

Electrochemical carbon capture and concentration (eCCC) offers a promising alternative to thermochemical processes as it circumvents the limitations of temperature-driven capture and release. This review will discuss the history of eCCC and transition towards discussing more recent approaches. For each approach, the achievements in the field, current challenges, and opportunities for improving these technologies will be described. This review is a comprehensive survey of the eCCC field and evaluates the chemical, theoretical, and electrochemical engineering aspects of different methods to aid in the development of modern economical eCCC technologies that can be utilized in large-scale CCS processes.

TOC Graphics:

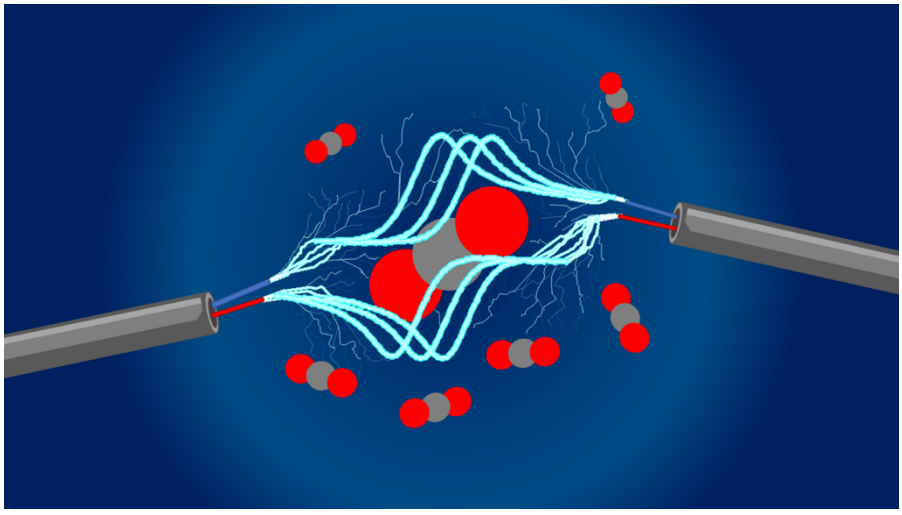

Table of Contents

1. Introduction.

Burgeoning population and industrialization have resulted in significantly increased global energy demand and fossil fuel consumption. As a result, anthropogenic carbon dioxide (CO_2) emissions have quickly grown to unsustainable levels. Despite aggressive targets and policies implemented globally to reduce emissions over the last several years, our annual rate of net CO_2 released has reached record levels, exceeding 36 Gt CO_2/year from fossil fuels and industry in both 2019 and 2021.[1-3] To limit global temperature rise to well below 2°C, as called for by the 2015 Paris agreement,[5] rapid and widespread decarbonization efforts are needed across all sectors of our economy.

In 2020, the power (i.e., electricity, heat) and industrial (e.g., cement production, chemicals/petrochemicals manufacturing) sectors accounted for over 50% of total emissions worldwide.[6] Within these sectors, large scale stationary "point-sources" make up the majority of these emissions, which are generated from burning fossil fuels or as chemical process byproducts.[7] The remaining generators of CO_2 emissions consist of small, disperse, and often mobile sources, primarily from the transportation, waste, and agricultural sectors.[2, 6, 8] The transition towards decarbonizing all of these sectors will need to be driven by a significant expansion of renewables and electrification, coupled with energy efficiency improvements. However, pathways towards decarbonization also call for large scale carbon capture and storage (CCS) or utilization/conversion (CCU). The proposed suite of carbon capture technologies can specifically address emissions from existing fossil-fuel based infrastructure, account for hard-to-decarbonize sectors (e.g., industrial byproducts), and enable net-negative applications.[1 9, 10]

Considerable progress has been made in the development and optimization of carbon capture systems, particularly for coal and natural gas power plant applications.[1] According to the Global CCS institute, more than 100 commercial scale CCS facilities are operational, in construction, or in development stages as of 2021, most of which capture CO_2 from the power and industrial sectors.[11, 12] However, in order to meet the Paris agreement, not only would all "point-source" processes need to approach net-zero carbon emissions, but emissions from other distributed sources also need to be significantly reduced or eliminated.[13] Direct air capture (DAC) of CO_2 represents a carbon-negative technology that could further act to lower emissions from non-point-source emitters.[14, 15] There are currently fewer commercialized DAC processes (19 plants operating worldwide), and those that do exist are relatively small-scale, although DAC is currently receiving increased levels of attention and monetary support from both public- and private-sector organizations.[16]

Despite the role CCS is project to play in emissions reduction, a major drawback to current technologies is that carbon capture and concentration (CCC) methods remain energy-intensive and costly, preventing widespread implementation.[17-21] One of the most mature CCC technologies is the utilization of amine-based absorbent solutions for capture from power plant flue gas. Such a process exploits the natural affinity of amines for absorbing CO_2 at room temperature, followed by the thermal regeneration of the absorber to enable cyclic use.[22] A weakness of this approach, and thermally driven separation in general, is the Carnot limitation incurred by the temperature swings necessary for absorption and desorption. As a result, a typical alkanolamine capture process operating between ~37–117 °C can only approach a maximum of ~21% energetic efficiency.[23] After decades of research, most state-of-the-art amine capture systems still have high heating demands of > 2.3 GJ/ton CO_2 (>110 kJ/mol CO_2). Therefore, current systems are limited to ca. < 20% of the Carnot efficiency, or < 5% overall energetic efficiency, upon optimization at scale.[24-27] To put this efficiency into context, 20–30% of the entire power output of a typical coal-fired power plant would be required to power a retrofitted CCC process alone.[28, 29] Using these systems, every ton of captured CO_2 would cost an estimated $50-100 for power generation plants and $40-120 for industrial sources (i.e., cement, iron, or steel).[30-33] CCC systems for DAC are further underdeveloped, and the heating demands are much higher due to the significantly lower CO_2 concentrations. Typical thermochemical DAC systems require > 5 GJ/ton CO2 (or > 240 kJ/mol CO_2), operating at < 10% of the energetic efficiency, resulting in higher system costs; however, it is important to note that due to the early development stage of DAC technologies, these energy estimates are generated with less certainty than point-source capture facilities.[18, 34] Reported DAC cost estimates are in the range of $130–1000/ton CO_2, dependent upon the source of heat to drive regeneration (i.e., waste heat or generated heat) and the carbon footprint associated with this heat.[18, 33-36] Specifically, methods which fall on the lower end of this cost range typically assume access to a source of waste heat to carry out process heating needs. Reaching net-zero emissions by 2040 is estimated to require about 2,000 large-scale CCS facilities worldwide.[37] While most current commercial demonstrations primarily use thermochemical approaches, achievement of large-scale carbon capture will likely require a diverse portfolio of options. Development of methods which offer higher energetic efficiencies than thermally-driven processes and are operated with low-carbon energy sources could enable more widespread deployment of CCC.

More efficient CO_2 separation strategies would specifically enable operation closer to the thermodynamic minimum for system energy requirements. To separate a species from a gaseous mixture, the minimum energy is equal to the difference in Gibbs free energy before and after separation. In the

limit of "skimming", where an infinitesimal quantity of CO_2 is removed from a feed gas mixture at ambient pressures, the Gibbs free energy of separation (ΔG) is given by Equation 1.[38]

$$\Delta G = -RT \ln\left(\frac{P_{CO_2}}{P_0}\right) \qquad \text{Eq. 1}$$

where R is the ideal gas constant (8.314 J mol^{-1} K^{-1}), T is the absolute temperature (K), P_{CO_2} is the partial pressure of CO_2 in the feed gas mixture, and P_0 is the ambient pressure. The relationship between the change of free energy and partial pressure demonstrates that CO_2 separation is an endergonic process whose energetics depend on the reaction conditions as well as the required changes in concentration. For example, for DAC, separating 400 ppm CO_2 from air at standard temperature (T = 298.15 K) and pressure (1 bar) to generate a pure CO_2 stream at 1 bar will require at least 19 kJ/mol CO_2. However, concentration from a flue gas stream containing 15 mol% CO_2 at ambient conditions requires a minimum work of separation of 4.7 kJ/mol CO_2. Note that "skimming" considered in Equation 1 represents a lower bound of energy requirements, which will increase with the fraction of CO_2 removed from the feed gas. Considering 90% removal of CO_2 from a flue gas mixture (15 mol% CO_2), and using expressions demonstrated in previous work,[18, 38] at least 6.4 kJ/mol CO_2 is required. The minimum thermodynamic work constitutes a limit which is unachievable under practical conditions due to irreversible losses (e.g., entropic losses); however, all processes, whether they are thermochemical, electrochemical, or otherwise, aim to balance these losses with process efficiency, selectivity, and yield, with a goal of minimizing cost.

Electrochemical carbon capture and concentration (eCCC) offers a promising alternative to thermochemical processes as it circumvents the limitations of temperature-driven capture and release.[39-43] More specifically, electrochemical carbon capture systems are not bounded by Carnot efficiencies, and can theoretically approach operation at the thermodynamic minimum energy requirement (i.e., 100% energetic efficiencies).[41] As such, in electrochemical systems, the minimum cell potential (E_{cell}) is related to the minimum separation work (represented by the change in Gibbs free energy).

$$E_{\text{cell}} = -\frac{\Delta G}{nF} \qquad \text{Eq. 2}$$

where n is the moles of electrons transferred per mole of CO_2 captured, F is the Faraday constant (96485 C mol^{-1}), and together, they describe the charge transferred during the reaction. As CO_2 separation is a nonspontaneous process ($\Delta G > 0$), the cell potential, or difference between the potential of the cathode and anode, is negative ($E_{\text{cell}} < 0$). This minimum cell potential is directly related to the relative CO_2 concentrations at the two electrodes via the Nernst equation. To perturb the reaction equilibrium and drive the process toward favorable CO_2 separation, the actual cell potential must be greater than $|E_{\text{cell}}|$,

resulting in energetic losses. This deviation from E_{cell} is dependent on the thermodynamic cycle of the separation system and overpotentials that result from resistive losses in the electrochemical cell(s). These cell resistances arise from a summation of inefficiencies associated with kinetic, ohmic, and transport phenomena that underlie system operation and their magnitudes are influenced by the chosen cell materials and reactor operating conditions (i.e., current density). Thus, cell potential and associated energy requirements are influenced by several design and operational factors. Despite these potential energetic penalties, an advantage of electrochemical systems is their ability to apply electric currents (via polarized electrode surfaces) that directly act on target redox-active molecules rather than on the entire capture medium via heating and cooling, thus reducing or eliminating sensible heat losses. Due to these differences in process energetics, electrochemical systems can potentially operate with reduced energy requirements over thermochemical systems and are therefore particularly attractive. Additionally, eCCC systems present an opportunity to operate at milder conditions (i.e., at or near room temperature), allow for modular designs that can more readily be scaled up or down, and can run on electricity from renewable sources.

This review will begin by discussing the history of eCCC, describing early work in the field and the motivation for pursuing such a process. We will then transition towards discussing more recent approaches, with a heavier emphasis on methods that employ redox mediators to facilitate CO_2 capture and release. These methods rely more on optimization through chemical design and include pH-mediated systems (Section 3), electrochemically-mediated amine regeneration (Section 4), and direct capture with redox-active molecules (Section 5). For each approach, we provide a general overview of the system, discuss redox mediator chemistries that have been studied in literature, and highlight requirements for future generations of redox mediators. We also describe previous demonstrations of each method and current cell/system designs that have been used at the lab-scale. To conclude (Section 6), we summarize achievements in the field, current challenges, and opportunities for improving these technologies. Overall, this review is a comprehensive survey of the eCCC field and evaluates the chemical, theoretical, and electrochemical engineering aspects of this approach. We hope this work can be used to assist the community in the development of modern economical eCCC technologies that can be utilized in large-scale CCS processes.

2. History of eCCC: Early work and Motivation.

Electrochemical carbon dioxide capture uses electron transfer reactions to capture and concentrate carbon dioxide. The original motivation for using an electrochemical approach to CCC can be traced back

to 1969, when Huebscher and Babinsky were interested in developing an efficient way to separate carbon dioxide from the atmosphere to be used for life support systems, specifically for use in submarines as well as air and space travel.[4]

The system design can operate continuously and includes two electrochemical concentration cell stacks, a process air blower, and a dehumidifying-humidifying unit (Figure 1). The process of CO_2 separation can be broken down into two stages, which are both typically operated at temperatures of 65°C or lower. The first stage (Stage I, Figure 1) features the carbonation cell, in which a CO_2-rich air stream (0.6%) is supplied to the cathode, where both CO_2 and oxygen (O_2) are removed (Scheme 1, cathodic reactions). Then, a concentrated mixture of CO_2 (66.7%) and O_2 (33.3%) is generated at the anode (Scheme 1, anodic reactions).

Scheme 1. Reactions governing Huebscher and Babinsky's low-temperature carbonation cell.[4]

Cathodic Reactions	**Anodic Reactions**
$O_2 + 2H_2O + 4e^- \rightarrow 4OH^-$	$HCO_3^- \rightarrow CO_2 + OH^-$
$CO_2 + OH^- \rightarrow HCO_3^-$	$CO_3^{2-} + H_2O \rightarrow CO_2 + 2OH^-$
$HCO_3^- + OH^- \rightarrow CO_3^{2-} + H_2O$	$4OH^- \rightarrow O_2 + 2H_2O + 4e^-$

Since the first stage captures both oxygen and carbon dioxide, the second stage (Stage II, Figure 1) is used for their separation. The cell is similar to the carbonation cell in Stage I, but it uses an acidic electrolyte such that oxygen is reduced at the cathode and reacts with protons to form water (i.e., $O_2 + 4H^+ + 4e^- \rightarrow 2H_2O$). During this reduction step which removes oxygen, CO_2 can be recovered at high purities. At the anode of the Stage II cell, water decomposes via oxidation to reform oxygen and protons (H^+); the O_2 is transferred out of the cell, and the protons are re-consumed at the cathode.

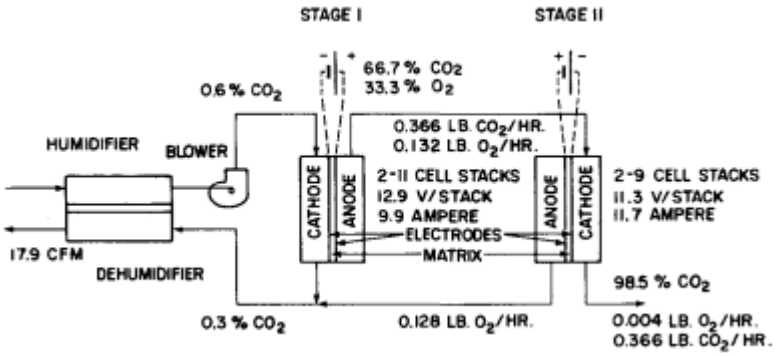

Figure 1. Huebscher and Babinsky model for the first known eCCC system. From ref 42 Reprinted with permission from SAE International.

This system captured CO_2 from low levels with concentration at high purities (97–98%) and was stable for over 1000 hours of operation. Additionally, this system was similar or lighter in weight than other systems at the time,[44,45] making it an effective option for mobile applications. However, the process is energy intensive, requiring cell voltages ca. ≥1 V for both stage I and stage II. This voltage is quite high, considering that the minimum cell voltage for separating 0.6% CO_2 is ca. 0.1 V (from eq. 1 and 2). Despite these limitations associated with Huebscher and Babinsky's system, it was the first demonstration of electrochemical CO_2 capture and concentration.

Later, in 1971, Wynveen and Quattrone used an ambient-temperature eCCC system for aircrafts,[46] which was also demonstrated by Wynveen et al. for spacecrafts.[47] Winnick et al. also explored the use of this system for O_2 regeneration during manned space missions using carbon capture, concentration, and conversion.[48] Wynveen and Quattrone's technology contained electrochemical cells operating continuously in series, where each used an aqueous cesium carbonate (Cs_2CO_3) electrolyte. The electrodes were made of a fine mesh onto which Teflon and platinum were cast, forming a porous platinum electrode. The setup was similar to that of a fuel cell, where the cathode and anode were separated by

Scheme 2. Reactions Governing Wynveen and Quattrone's Low-Temperature Carbonation Cell

Cathode Reactions	**Anode Reaction**
$O_2 + 2H_2O + 4e^- \rightarrow 4OH^-$	$2H_2 + 4OH^- \rightarrow 4H_2O + 4e^-$
$CO_2 + OH^- \rightarrow HCO_3^-$	$CO_3^{2-} + H_2O \rightarrow HCO_3^- + OH^-$
$HCO_3^- + OH^- \rightarrow CO_3^{2-} + H_2O$	$HCO_3^- \rightarrow CO_2 + OH^-$

the electrolyte (supported by a porous matrix), and gas-phase reactants were fed directly to the electrodes. The feed gas on the cathode side is humid, CO_2-containing cabin air. The cathode had a similar function to the Stage I cathode of the Huebscher and Babinsky method described above (Scheme 1), where both CO_2 and O_2 are reduced and thus captured. On the anode side, hydrogen is fed to the cell,

which is oxidized, reducing the solution pH, leading to the dissociation of either bicarbonate ions or carbonic acid into CO_2 (similar to the anode reaction of Scheme 2).

A major problem associated with this system was the poor ionic selectivity of the electrolyte-imbibed porous matrix used to separate the electrodes. The architecture was improved by Eisaman et al. by the use of anion exchange membranes,[49] but the current density of the CO_2 concentrator was low (0.5 mA cm^{-2}) and the system required a particularly high humidity in order to prevent electrolyte precipitation. Additionally, the energy required to run the process was 350 kJ/mol CO_2 for separation from air, which is significantly higher than the minimum separation work, yielding low energetic efficiencies.

2.1 High Temperature Molten Cell Electrolyzers.

Carbonation cells for CO_2 capture, as described in Section 2.1 in the context of low temperature applications, can also be operated at higher temperatures. These technologies have adapted molten carbonate fuel cell platforms for carbon capture and concentration (i.e., driven mode), with some methods also using schemes that can generate energy simultaneously (i.e., fuel-cell mode). Compared to the low temperature carbonation cells, which use aqueous-based electrolytes, these devices employ molten salt electrolytes. This enables lower sensitivity to feed-gas humidity and higher conductivity, and in previous demonstrations, allowed for higher current densities with either similar or improved system efficiencies. The higher temperatures also improve electrode kinetics, which can reduce the need for noble metal catalysts.[50, 51] The reaction mechanisms are similar to that described for low-temperature carbonation cells in Section 2.1, where CO_2 is consumed at the cathode and discharged at the anode, but the cells are run at much higher temperatures (≥500°C). Kang and Winnick demonstrated a molten carbonate CO_2 capture device in a driven mode, where CO_2 was concentrated from 1% to 5.8% and 0.25% to 3.4% in a lab-scale cell.[52] The low CO_2 concentration at the anode was due to use of a nitrogen sweep gas to collect the released CO_2; therefore the level of CO_2 concentration at the anode is expected to be higher in a more optimized and scaled up device. However, similar to low temperature devices, this type of cell is limited in its ability to recover CO_2 at high purities due to the simultaneous production of O_2 at the anode (as described in Scheme 1). Additionally, to keep the molten carbonate electrolyte from decomposing, the voltage range was limited, which also limited accessible current densities in this demonstration.

3. pH-Mediated eCCC Systems

3.1 Overview

Electrochemically generated pH changes in aqueous solutions presents a particularly unique approach for the absorption and release of carbon dioxide. Like other solvents, the concentration of physically dissolved CO_2 in water remains constant at a given temperature and pressure in accordance with Henry's law. Unlike other solvents, however, water readily reacts with dissolved CO_2 in solution to form a complex buffer consisting of carbonic acid, bicarbonate, and carbonate (eq. 3–5).

$$CO_{2(aq)} + H_2O \overset{K_1}{\longleftrightarrow} H_2CO_3 \quad \text{Eq. 3}$$

$$H_2CO_3 + OH^- \overset{K_2}{\longleftrightarrow} HCO_3^- + H_2O \quad \text{Eq. 4}$$

$$HCO_3^- + OH^- \overset{K_3}{\longleftrightarrow} CO_3^{2-} + H_2O \quad \text{Eq. 5}$$

The concentration and proportion of these species is dependent upon the solution pH. At high pH, the reactivity of CO_2 with hydroxide results in a larger concentration of CO_2 to effectively be "stored" in solution in the form of carbonate or bicarbonate. Acidification of the solution reverses the buffer equilibrium and releases the captured gas. Recently, research groups have sought to exploit this characteristic of aqueous systems for the development of electrochemical CCC systems. Here, we provide a short overview of electrodialysis/electrodeionization systems and more extensively describe pH-swings with redox mediators. A more thorough description of electrodialysis/electrodeionization is provided in the recent review by Sharifian et al.[53]

3.1.1 Electrodialysis/Electrodeionization.

Bipolar membrane electrodialysis (BPMED) has been applied as one method for pH-mediated eCCC.[54] BPMED uses a combination of cation and anion exchange membranes and a current to separate a solution by charge. In aqueous media, the water molecules are split into protons and hydroxide ions to balance charge. Thus, using a sodium chloride (NaCl) electrolyte, the electrolyte separates into sodium hydroxide (NaOH) and hydrochloric acid (HCl). In the capture stage, CO_2 reacts with NaOH to form carbonate (specifically $Na_2CO_3 \bullet 10H_2O$), which can be removed through crystallization. The process can also be reversed to release concentrated CO_2.

BPMED has been studied for a variety of carbon capture applications. For direct air capture (~400 ppm CO_2), Eisaman et al. found that when using solutions of sodium or potassium hydroxide and applying a constant-current across a BPMED stack, it is possible to remove CO_2 with an energetic cost of about 200 kJ/mol CO_2; the regeneration of CO_2 using BPMED from carbonate requires an additional ~100 kJ/mol CO_2.[55, 56] Therefore, the entire process requires a minimum energy input of about 300 kJ/mol CO_2 to extract and recover carbon dioxide from the atmosphere. Sabatino et al. noted in their techno-economic

review that their direct air capture setup has an energy requirement as low as 236 kJ/mol CO_2, but a minimum cost of $773/ton CO_2 due to the high costs of bipolar and ion exchange membranes [57]

BPMED was also used to remove CO_2 from seawater, samples were run through a BPMED system to separate them into acidified and basified sea water solutions. The minimum total electrochemical energetic input for extracting 59% of the total CO_2 in solution was 242 kJ/mol, which was expected to improve with the scale-up of the BPMED to commercial-scale seawater capture systems.[58] Additionally, Carlson and coworkers attempted to capture CO_2 from flue gas using a combination of BPMED and electrodeionization.[59] This system effectively modulated the solution pH, and capture was achieved from a 15% stream to 80% CO_2.

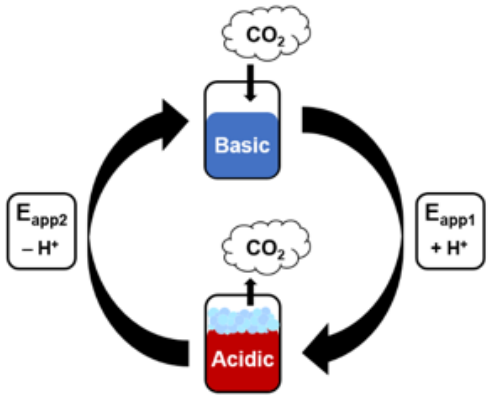

Figure 2. General representation of a pH mediated eCCC cycle.

3.1.2 pH swing with PCET mediators.

Other systems capitalize on pH changes by using redox-active proton mediators. Compounds capable of proton coupled electron transfer (PCET) have the potential to be particularly useful for pH-swing eCCC processes, which utilize an electrochemical bias to shift pH in one direction or the other to facilitate CO_2 capture or release. In a typical system, a CO_2-containing feed stream is contacted with a basic solution and captured in the form of dissolved inorganic carbon (HCO^{3-}, $CO3^{2-}$, and $CO_{2(aq)}$). To release the captured gas, a potential is applied (E_{app1}, Figure 2) to oxidize the mediator, which consequently undergoes deprotonation. Acidification due to mediator deprotonation shifts the equilibrium to favor CO_2 evolution. To regenerate the basic solution, a more negative potential (E_{app2}, Figure 2) is applied to reduce, and consequently protonate, the mediator. The resulting increase in solution basicity promotes CO_2 capture via dissolved inorganic carbon formation, completing the overall cycle.

For efficient CO_2 separation via pH-swing eCCC, an ideal PCET redox mediator should be highly soluble and have a sufficiently high pK_a difference in its reduced/oxidized forms to generate large pH changes adequate for CO_2 capture and release. The mediator must also be stable under both acidic and alkaline conditions for extended periods of time. Additionally, these molecules must exhibit stability in the presence of the feed gas composition of interest. For example, air contains high concentrations of oxygen, and thus the mediator must be O_2-stable in these DAC applications. Lastly, mediators capable of concerted proton-electron transfer (CPET) reactions are beneficial as they can enable operation at milder

potentials.[60] Several classes of molecules have been identified as candidate redox mediators for pH-swing driven eCCC, including quinones,[61-68] phenazines, [69, 70] redox-active amines,[71] inorganic compounds, [61,72] and even a riboflavin compound.[73]

3.2 Demonstrations.

3.2.1 Quinones.

Quinones are a well-studied family of molecules that have been shown to readily undergo 2 H^+, 2 e^- PCET reactions to interconvert between their quinone and hydroquinone forms (Scheme 3).[74, 75] Reduced quinones have also been used directly to capture CO_2 in aprotic conditions, as described in Section 5. In this section, their use in pH-swing cycles will be discussed. The ubiquity of quinones in nature and other fields of research have led to a large catalogue of commercially available or readily accessible derivatives that span an extensive range of measured redox potentials and solubilities.[61-63] Additionally, many quinones undergo PCET reactions in aqueous solutions with facile conversion between quinone and hydroquinone forms.[74] Unfortunately, most commercially-available quinones have limited solubility and stability in aqueous solutions, confining the current landscape of suitable candidates to only a handful of examples.[64-66] However, these types of properties can be improved with molecular functionalization.[67] Huang et. al. reported the utilization of tiron (disodium 4,5-dihydroxy-1,3-benzenedisulfonate, an ortho-hydroquinone) as a redox-active pH mediator to successfully capture and release carbon dioxide from simulated flue gas streams.[62] In a proof-of-concept demonstration with 0.7 M quinone concentration in solution, the pH was changed between 9.2 and 5.7 using constant current electrolysis at 18 mA cm^{-2}. The system was generally effective, operating at >90% Faradaic efficiency, and the estimated energy requirements were similar to existing thermally-driven systems (2.4 GJ/ton CO_2 or 105.6 kJ/mol CO_2). However, a nitrogen sweep gas was used in this demonstration to remove desorbed CO_2, which is unrepresentative of expected system operation where CO_2 is collected at high concentrations. Thus, energetic and Faradaic efficiencies are expected to be lower than these reported values under more realistic operating conditions. However, the experiment was run in a non-optimized H-cell platform, and performance would be expected to decrease as the cell and overall system are

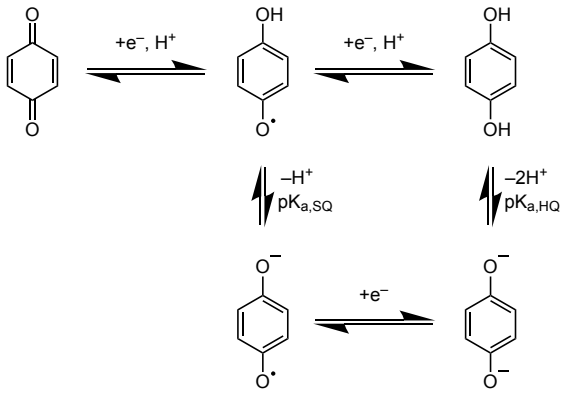

Scheme 3. Quinones can undergo two separate one-electron reductions in the presence of a proton source to form the semiquinone (SQ) and the hydroquinone (HQ).

engineered for higher performance. Another challenge with this PCET chemistry is its long-term stability; the system was unable to perform multiple capture-release cycles, limiting its practicality.

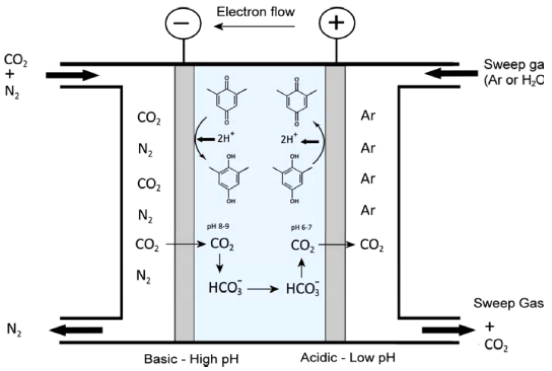

Figure 3. General representation of a membrane-supported polymer system developed by Watkins et al. in ref. 65. Figure used with permission from the American Chemical Society.

Watkins et al. explored a different system, where 2,6-dimethylbenzoquinone was used as the pH mediator of choice and was employed in a gas-fed electrolyzer.[68] In their system, a porous separator was soaked in the liquid electrolyte solution containing 10 mM 2,6-dimethylbenzoquinone and 10 mM of the equivalent hydroquinone and supported between two gas diffusion electrodes (depicted in Figure 3). In their system, the liquid electrolyte saturated separator works in conjunction with metal catalyst-coated electrodes to effectively drive a pH gradient across the cell. Using platinum (Pt) deposited electrodes, CO_2 was selectively transported from the feed gas side of the cell (cathode) to the collection side of the cell (anode). They demonstrated CO_2 removal at the cathode and recovery at the anode from a simulated flue gas stream (14% CO_2, 3% O_2, and 87% N_2) with no transport of other gases detected. Although no energetic efficiencies were reported, large cell voltages were applied (between 1–2.5 V for the Pt catalyst). Jin et al. estimated that the required energy of this experimental demonstration was ~600 kJ/mol CO_2.[76] Additionally, the low quinone concentrations that were used due to solubility issues limited the pH range and thus CO_2 removal efficiency.

3.2.2 Phenazines.

Phenazines are another promising family of redox-active pH-mediator compounds. Analogous to quinones, phenazines reversibly undergo 2 H^+, 2 e^- PCET reactions over a wide pH range. Sulfonated phenazine derivatives have also displayed high aqueous solution solubilities and stabilities. Jin et al. demonstrated use of 3,3'-(phenazine-2,3-diylbis(oxy))bis(propane-1-sulfonate) in a pH-swing system for carbon capture.[69] In the absence of CO_2, the pH was increased from 4 to 13.4 using 0.1 M phenazine concentration, and then cycled between a pH of 13.4 and 7.5 over four total cycles. When a continuous flowing stream of a CO_2/N_2 mixture (CO_2 partial pressure of 0.465 bar) was contacted with the electrolyte, they observed a decrease in CO_2 partial pressure down to ca. 0.38 bar following deacidificiation and an increase up to ca. 0.57 bar following acidification. They cycled using a stream of 100% CO_2 during the desorption step to simulate more realistic operating conditions, where CO_2 must be released and

concentrated to high purities. For their system set-up, Jin et al. estimated from thermodynamic calculations that a minimum of 16–75 and 30–75 kJ/mol CO_2 is required for capture from 10% and atmospheric CO_2 sources, respectively (8–35% and 27–67% energetic efficiency, respectively). Comparatively, experimental data indicates that their system can separate carbon dioxide from a mixture containing ca. 46.5% CO_2 with energy requirements in the range of 49–120 kJ/mol CO_2, depending on the operating current density. One limitation of this system, and pH-mediated processes for eCCC in general, is slow CO_2 absorption kinetics. In their specific demonstration, CO_2 absorption had to be continued for roughly 40 minutes after completion of electrochemical deacidification.

In another recent study, Xie et al. utilized a series of phenazine PCET pH-mediators in a continuous flow eCCC setup (Figure 4).[70] They identified 7,8-dihydroxyphenazine-2-sulfonic acid as the most effective phenazine derivative. Using a 25 mM phenazine concentration, capture from a simulated flue gas composition (15:85 CO_2:N_2) with an estimated energy consumption of 0.49 GJ/ ton CO_2 (22 kJ/ mol CO_2) and Faradaic efficiency >95% was performed. Their estimated energetic efficiencies are highly competitive with other CCC approaches, surpassing state-of-the-art amine capture systems.[28, 29] However, CO_2 release during desorption was measured using a N_2 or argon (Ar) carrier gas, which is not representative of a real system where carbon dioxide is released and concentrated to high CO_2 concentrations. Thus, energy requirements will be higher and Faradaic efficiencies will be lower than reported values in the study. Their system displayed high stability in the presence of CO_2 and N_2 over the tested time-scale; Xie et al. estimated a capacity retention of 97.9% over 8 capture-release cycles. However, they anticipate that this phenazine compound may be O_2-sensitive, which could significantly reduce its effective stability under practical conditions.

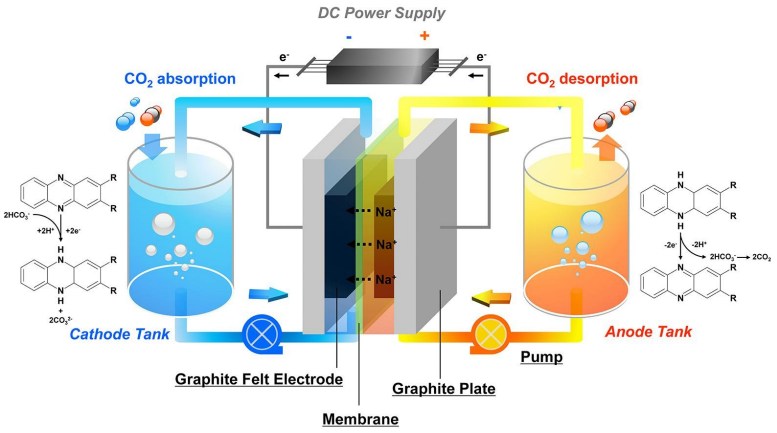

Figure 4. Continuous flow eCCC system featuring phenazine PCET pH-mediators reported by Xie et. al. Figure used with permission from Ref. 67.

The same group (Xie et al.) has more recently demonstrated the use of the proton-carrier riboflavin 5'-monophosphate sodium salt hydrate at a concentration of 25 mM in aqueous solution as a PCET pH-mediator in these types of systems.[73] In a similar set-up, they demonstrated CO_2 capture from a 15:85

CO_2:N_2 flue gas stream, with estimated energy requirements of 9.8 kJ/mol CO_2 (~48% efficiency) and Faradaic efficiencies of >93%. Similar to their previous study, they used a carrier gas (N_2 or Ar) during desorption. Therefore, expected energy requirements and Faradaic efficiency under more practical operation is currently unclear for this system. This chemistry exhibited relatively good stability in the N_2/CO_2 environment, with 0.39% capacity fade per cycle measured over 21 total cycles; however, O_2 stability was not reported. One current limitation of this riboflavin derivative is its low solubility, which limits redox-mediator concentration and thus quantity of CO_2 that can be separated in each cell.

3.2.3 Redox-Active Amine.

Hatton and coworkers recently investigated a system that uses a redox-active amine for capture via pH swing. Cationic 1-aminopyridinium nitrate was identified as a redox-active pH mediator as it furnishes a reversible redox couple in water. An aqueous 0.2 M 1-aminopyridinyl solution was reduced in the presence of N_2, then exposed to 100% CO_2.[71] Full conversion to the radical had a 53% Faradaic efficiency with an estimated minimum energy consumption of 101 kJ/mol CO_2. However, the authors projected that reducing conversion can enable lower energy requirements. Notably, they studied the stability of the radical in an oxygenated atmosphere over a period of one month. The radical was not stable over long periods of time, leading to capacity decreases of 6.6 and 46% over 1 and 30 days, respectively. However, they also studied the radical in a nitrogen atmosphere and found that after 30 days, the capacity decreased to 55%. The authors conjecture that the radical may be reacting with itself to form 4,4'-bipyridine.

3.2.4 Inorganic Compounds.

In a different approach, Rahimi et al. proposed using manganese oxide (MnO_2) coated electrodes to act as heterogeneous PCET pH-mediators, according to eq. 6, for CO_2 capture.[61]

$$MnO_{2(s)} + H^+ + e^- \rightleftharpoons MnOOH_{(s)} \qquad \text{Eq. 6}$$

One benefit to this system is that manganese oxides and hydroxides (MnOOH) are highly stable at various pH values and MnO_2 readily undergoes PCET reactions in aqueous solutions.[72] In this system the pH mediator is immobilized on the electrode surface and requires batch-type operation, where the electrode polarity must be switched periodically to drive CO_2 capture and release via proton intercalation and deintercalation of the electrodes, respectively. A cell voltage of 1 V was applied, and polarity was switched every 2 hours for a total of 4 cycles (i.e., 8 hours), where ~0.4 mmol of CO_2 was captured and recovered each cycle. Energetic efficiencies where not reported; however, Rahimi et al. estimated with a simple modeling analysis that this pH-swing process could theoretically separate CO_2 from flue gas (15% CO_2) at an energetic cost of 33.2 kJ/mol CO_2 (~14% energetic efficiency).

3.3 Cell and System Design.

Current studies involving pH swings (and eCCC systems in general) mainly include proof-of-concept demonstrations with candidate chemistries, which are important in early-stage research. However, there is less research involving characterization of cell performance and optimization of experimental configurations. Transitioning towards higher performance pH-swing eCCC systems will require not only optimized redox mediator molecules, but also engineered cell/system designs which maximize CO_2 separation capacity and simultaneously minimize losses associated with kinetics, ohmics, and mass transport. Here we briefly review current experimental cell designs for electrochemical CO_2 separation processes which use a pH swing, to contextualize where the field is at and highlight key areas for future work.

A common experimental set-up employed for pH-swing systems resembles a redox-flow battery (RFB) (shown in Figure 4). Both Xie et al. and Jin et al. used this type of set-up to test their phenazine and riboflavin chemistries, as previously described.[77,70, 73] This type of system is comprised of a flow cell, two reservoir tanks to contain the positive and negative electrolytes (7-50 mL), respectively, and pumps to circulate the working and counter electrolytes through the cell (Xie et al. reported using electrolyte flow rates of 200 mL min^{-1}).The cell design employs porous carbon electrodes (typically paper, cloth, or felt) and engineered flow fields to deliver the electrolyte solution to the electrode. A membrane or separator is used to physically separate the two electrodes while enabling ions (e.g., Na^+ or K^+) to exchange between the electrolytes to maintain electroneutrality. This setup operates in a cyclic fashion (charge / discharge cycles), applying a current or cell voltage to deprotonate the mediator, then switching the direction of current flow or electrode polarity to protonate the mediator. CO_2-containing feed gas (or sweep gas) is then contacted with the liquid electrolyte in the working-side reservoir during and/or after the protonation (or deprotonation) half-cycle to enable CO_2 capture (or removal). Xie et al. used 4 cm^2 (geometric/projected area) graphite felt electrodes, serpentine or flow-through flow fields, and a Nafion 115 or 117 cation exchange membrane in their experiments.[70, 73] Their cell was operated with applied current densities of 10–30 mA cm^{-2}, resulting in average cell voltages of ca. 0.06–0.2 V. While these low voltages led to low energy requirements, the experimental system requires validation with a pure CO_2 sweep gas at the anode to understand performance under more realistic operating conditions. Additionally, a key engineering challenge for this cell set-up in its current form is a relatively high ohmic resistance (2.48 Ω or 9.92 Ω cm^2 measured with EIS), which may induce large energetic penalties and/or limit achievable current densities.[70] Jin et al. reported a flow cell consisting of a Fumatech cation exchange membrane (E-620(K)) and 5 cm^2 electrodes (although the electrode and flow field type were not

specified).[77] The cell was operated galvanostatically at 50 mA cm^{-2} with potential holds at the end of each half-cycle. Cell performance metrics (i.e., overpotentials or resistances) and challenges associated with this set-up were not directly discussed.

Watkins et al. employed a different cell configuration, similar to a fuel cell, to test solubilized quinone mediators.[68] The system utilized a gas-fed electrochemical reactor (shown in Figure 3 above) which could operate in a continuous fashion. As described previously, the cell contained catalyst-coated gas diffusion electrodes and an electrolyte imbibed separator. Their electrodes consisted of Sigracet 25 BC carbon paper with a hydrophobized microporous layer (MPL), and they applied a catalyst layer on top of the MPL. Their separator was a hydrophilic porous polypropylene material (Celgard 3501), which was soaked in liquid electrolyte before assembling and running the cell. The liquid electrolyte was an aqueous solution consisting of 10 mM of the quinone, 10 mM of the hydroquinone, and 1 M $NaHCO_3$ which served as both the sorbent and supporting salt. Flow fields (25 cm^2) were employed to distribute and remove gases to and from the electrodes. Gases that were fed to their system on the capture (cathode) and release (anode) sides were pre-humidified, which is typically done in low-temperature fuel-cell technologies to prevent the membrane/separator from drying out. Watson et al. explored the use of platinum, palladium, and ruthenium catalysts, and found that platinum enabled the greatest CO_2 concentration change and suppressed water splitting across a range of cell potentials (1–2.5 V). Cell voltage requirements were high for this system compared to the approaches mentioned above, without a clear understanding of what phenomena contributed to this inefficiency (e.g., ohmic resistance, mass transport, etc.).

The MnO_2-based technology of Rahimi et al. makes use of immobilized rather than solubilized pH mediators. In their demonstration, they used a liquid flow-based setup to test their MnO_2 mediator system. The platform was similar to the RFB-type systems described above, consisting of an electrochemical cell to drive protonation/deprotonation, reservoir tanks to hold liquid electrolyte for the working and counter sides of the cell, and pumps to circulate electrolyte between the cell and reservoirs. Their liquid-fed cell consisted of 25.8 cm^2 carbon cloth electrodes (AvCarb) coated with MnO_2 particles, parallel flow channels to deliver electrolyte to the electrodes, and a Selemion AMV anion exchange membrane.[61] The flow channels also contained plastic baffles to promote turbulence and enhance mass transport by specifically disrupting boundary layer growth, preventing channeling, and increasing local velocity.[78] Fabrication of the MnO_2 electrodes was demonstrated using two separate methods. The first was a casting method, where MnO_2 powder was synthesized using co-precipitation, and then a slurry containing this active species was cast onto a carbon-based, porous substrate.[79, 80] The second method involved electrodeposition of MnO_2 onto the substrate, which was shown to achieve more uniform

deposition and higher capacitance (specific and geometric). Due to the use of redox mediators immobilized on the electrode surface, the cell must be operated in a batch mode, where polarity is switched in cycles to prevent the complete proton saturation and depletion of the electrodes, respectively. In this study, the cell adopted a symmetric format with identical electrodes on either side, and the experiments were also started with the same electrolyte concentrations. During each half-cycle, the cell was operated with a constant applied potential of ±1 V, while the measured current density varied within the range of ±0–2 mA cm^{-2}. Absorption or desorption of CO_2 was carried out in a separate step following each electrolysis half-cycle by contacting the electrolyte with the feed or sweep gas. Overall, the current cell format operated with high cell voltages and low operating current densities, and thus, cell optimization work would be beneficial.

4. Electrochemically Mediated Amine Regeneration (EMAR).

4.1 Overview.

As previously described, one of the most investigated methods for CO_2 capture from power plant flue gas uses amine absorbents. The standard amine used for this method is monoethanolamine (MEA) since it has a high rate of CO_2 absorption, easy regeneration, and low replacement cost.[81] In this process, the flue gas is bubbled through the amine solution in the absorber, where the amine effectively captures CO_2 to form a carbamate. To release the CO_2, the carbamate solution is heated (~110°C for MEA) in order to thermally break the amine-CO_2 bond.[82] The released CO_2 is concentrated and collected. However, there are challenges with this traditional regeneration process, including low energetic efficiencies and degradation of amines at high temperatures. Thus, the operational temperature must be high enough to break the bond with CO_2, but low enough that the amine does not degrade. As a result, the temperatures used for the desorption process are not extreme enough to fully liberate the CO_2 bound to amines and typically only half of the bound gas is released.[83] Additionally, the narrow temperature range decreases the achievable energetic efficiency of the process due to greater Carnot limitations. In order to increase the efficiency of CO_2 release, methods other than temperature swings have been investigated.

Electrochemically mediated amine regeneration (EMAR), developed by Hatton and co-workers, is a promising alternative to temperature swing amine regeneration. EMAR relies on the use of an absorbent blocker that is electrochemically activated and deactivated to induce the release of covalently bound CO_2 from the amine. This process still capitalizes on the affinity of amines for binding CO_2. However, when the blocker is activated, it will preferentially bind to the amine and displace CO_2 from the carbamate.[82-84] Since

amine regeneration in EMAR is not temperature-driven, where the desorption temperature is limited due to thermal amine degradation, it can potentially liberate 80 to 90% of the absorbed CO_2.

The success of EMAR relies on the difference between binding constants of the amine-CO_2 and amine-

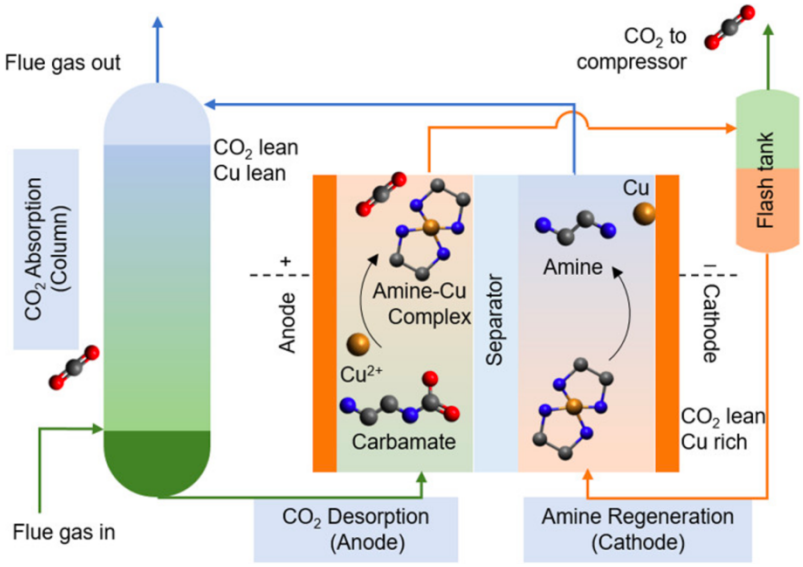

Figure 5. EMAR cycle in which an amine-based solvent is brought into contact with simulated flue gas to form carbamate. The carbamate-rich amine-based solvent is pumped to the anodic compartment. Upon electrochemical oxidation, Cu^{2+} is introduced to the solution, and the Cu–amine complex forms, releasing CO_2. The gas phase is separated, and the Cu–amine solution is pumped back to the cathodic compartment where Cu^{2+} ions are electrochemically plated onto the electrode, releasing—and, hence, regenerating—the amine. Reprinted with permission from the American Chemical Society from ref 79.

blocker complex. The amine and blocker should form a stable complex with the equilibrium constant that is much larger than that of the amine with the CO_2. The standard blocker and amine used in EMAR are copper and ethylenediamine (EDA). These species both fit the designated requirements, such that once Cu^{2+} is present in solution the amine will release CO_2 in favor of binding to copper. The equilibrium constants for EDA with CO_2 and Cu^{2+} are given below [82, 84]

$$2\mathrm{EDA(aq)} + \mathrm{Cu^{2+}} \overset{K_{Cu}}{\rightleftharpoons} \mathrm{Cu(EDA)_2^{2+}} \qquad K_{\mathrm{Cu}} = 2.10 \times 10^{18} \qquad \text{(Eq. 7)}$$

$$\mathrm{EDA(aq)} + \mathrm{CO_2(aq)} \overset{K_{CO_2}}{\rightleftharpoons} \mathrm{EDA(CO_2)(aq)} \qquad K_{\mathrm{CO_2}} = 4.90 \times 10^{4} \qquad \text{(Eq. 8)}$$

The EMAR process is similar to the temperature driven amine-based solvent system, except the desorber is exchanged with an electrochemical cell (Figure 5).[82] EMAR begins with contacting flue gas with the amine solution in an absorber, where the CO_2 reacts to form a carbamate. The carbamate solution then flows to the anode of the electrochemical cell where copper (Cu^0) is oxidized to Cu^{2+} and dissolved into solution. The amine preferentially binds to Cu^{2+}, liberating the CO_2, which is then collected. The copper-amine complex in solution is circulated back to the cathode of the electrochemical cell where copper is reduced back to Cu^0 and plated onto the electrode, effectively regenerating the amine so the cycle can begin anew.[82-84]

4.2 Demonstrations.

In early work for the EMAR process, Stern et al. compared fourteen different amines that included monoamines, amino acids, and polyamines before narrowing the selection to just four polyamines - ethylenediamine (EDA), triethylenetetramine (TETA), aminoethylethanolamine (AEEA), and diethylenetriamine (DETA). Polyamines were selected as they are more likely to chelate copper ions with high binding constants to form stable copper complexes. The other ten amines had a tendency to precipitate as salts, especially in the presence of CO_2, making them unsuitable candidates.[85] The four polyamines were analyzed for their preference for Cu^{2+} in the presence of CO_2, CO_2 loading capacity, and open-circuit potential measurements. the amount of copper required to deactivate the amine was examined. It was found that for EDA, AEEA, and TETA, one equivalent of Cu^{2+} binds to each amine; however, this ratio for DETA depended on the copper loading (which is proportional to Cu^{2+} concentration). At higher copper concentrations, one DETA molecule binds to each Cu^{2+}, and at lower copper loading, two DETA molecules bind to each Cu^{2+}. meaning that more copper is required to deactivate the molecule and release CO_2. Commonly used amines theoretically have a CO_2 capacity of 0.5 as carbamate formation results in a zwitterion, where two amines are required for every molecule of captured CO_2 (See Section 4.4). TETA, AEEA, and DETA all showed loading below 0.5, which could be caused by unreacted secondary amine groups present in these three polyamines. EDA, which has no secondary amine group, possessed a loading slightly over 0.5 likely due to the formation of bicarbonate, a common side reaction for primary amines.[83] Lastly, the difference in the open-circuit potentials for a copper electrode under anodic and cathodic conditions was used to estimate the minimum energy needed for releasing and removing Cu^{2+} into solution. Here, the concentration of EDA and Cu^{2+} was identical at the two electrodes, and thus open-circuit potential differences arise from differences in CO_2 concentrations at the electrodes. After these initial tests, EDA was selected as the standard amine for use in EMAR due to its high CO_2 loading capacity (likely due to a lack of secondary amine groups). EDA has also been identified as a desirable candidate in the thermal-swing CO_2 capture systems; however, the heat required for CO_2 desorption from EDA is too high to be economically practical.[83]

Early bench-scale demonstrations of the EMAR system captured and concentrated CO_2 from a pure feed stream (100%) of CO_2 with an energy requirement of ≤ 100 kJ/mol CO_2 and Faradaic efficiencies up to 80%.[85, 86] Separation from streams with lower CO_2 concentrations was not performed in this early system, as the copper swing of their benchtop system (i.e., conversion between Cu^0 and Cu^{2+} in the electrochemical cell) was not high enough compared to the concentration of CO_2 physically dissolved in solution. Advances in the EMAR cell design have resulted in significant performance improvements, as

described in the following section. Additionally, more recent EMAR demonstrations have operated at an elevated fluid temperature (55 °C), which enhanced electron transfer kinetics at each electrode and reduce CO_2 solubilities during desorption.[87, 88,82] The current bench-scale process can capture CO_2 from a 15% CO_2 feed stream (N_2 balance), while operating at 40–80 kJ/mol CO_2.[87] The system has also demonstrated stable operation for 50 hours.

Liu et al. studied the use of MEA rather than EDA in a thermal-electrochemical co-driven system (TECS), where they essentially combined the more commonly used amine from thermally driven CO_2 capture and EMAR.[62] This system parallels the EMAR scheme described above (Figure 5), with MEA binding to CO_2 and then Cu^{2+} being introduced electrochemically; however, a thermal step is also used. After Cu^{2+} ions have been stripped and dissolved, the solution is heated to 90 °C to assist in the removal of CO_2 from MEA.[89] The additional heat is needed in TECS likely because the solubility of copper in MEA-based solutions is moderately low, leading to insufficient Cu^{2+} concentrations in solution to displace CO_2 in all of the MEA-CO_2 present.[84] One challenge Liu et al. encountered was the reduction of Cu-MEA—and thus the regeneration of Cu^0 and MEA—was slow. Adjusting Cu^{2+} concentration, CO_2 loading, temperature, and KNO_3 concentration of the system decreased the charge transfer resistance and improved kinetics. Further, increasing the Cu^{2+} concentration and temperature improved mass transfer and thus reduced the associated overpotential. A combination of data from experimental techniques (cyclic voltammetry, potentiodynamic polarization, and electrochemical impedance spectroscopy) and a regression analysis found that the optimum operating conditions for this TECS system are a Cu^{2+} molality of 0.25 mol/kg, CO_2 loading of 0.37 mol_{CO2} /mol_{amine}, a temperature of 90 °C, and KNO_3 molality of 1 mol/kg. Under these conditions, the regeneration energy consumption is predicted to drop to 1.3 GJ/t CO_2 (63 kJ / mol CO_2).[89] These conditions can enable higher energetic efficiencies than traditional amine regeneration processes, which typically require >2.3 GJ / ton CO_2 (>110 kJ / mol CO_2).[24-27] These efficiencies are also comparable to estimated energy requirements of Wang et al. for their lower temperature EMAR system (with EDA) of 40 – 80 kJ / mol CO_2.[87]

4.3 Cell and System Design.

The EMAR process, pioneered by Hatton and co-workers, is arguably the most developed redox-mediator-based method for eCCC in the peer-reviewed literature, as there have been several bench-top, flow-cell level demonstrations, as well as engineering assessments regarding cell design metrics.[66 70 83 85, 86, 87 90 91 84 90] In an early embodiment, the EMAR cell consisted of copper plate electrodes and a porous polypropylene separator (Celgard 3501) to physically separate the cathodic and anodic electrolyte solutions while maintaining an ionic connection. Liquid-phase reactants were fed to the cathode and

anode using parallel flow channels with a rectangular cross-section. As described above, early demonstrations with this flow cell captured CO_2 at ≤ 100 kJ/mol CO_2.[85, 86] This prototype cell had a relatively low operating current density (5 mA cm^{-2}) and was limited by low swings in copper loading (i.e., conversions), resulting in less than 1% of bound CO_2 being released per pass in the electrochemical cell.[85, 86,90]

Analysis of the EMAR cell using two-dimensional (2D), convection-diffusion modeling of the planar electrodes has suggested large mass transport limitations emerge with increased conversion per pass. Specifically, the model predicts the development of a thick boundary layer in the flow direction, which, in turn, leads to an increase in the cell voltage at relatively low current densities (<8 mA cm^{-2}), where the cell enters a mixed kinetic-mass transfer regime.[90] This limitation can be overcome by increasing the electrolyte flow rates, albeit at the expense of conversion per pass. Wang et al. estimate that current densities greater than 50 mA/cm^2 could be achieved with improved mass transport properties of the cell.[91] When tested with galvanostatic experiments (10 mA/cm^2), increasing the flowrate from 75 to 225 mL/min reduced cell voltage by 20%, albeit at the expense of Cu^0/Cu^{2+} conversion per pass and thus CO_2 separation capacity. Additionally, large baffles (a form of turbulence promoters) were incorporated into the flow channels of an EMAR cell, which led to a 25% reduction in cell voltage, similar to the effect of increasing flow rate but without decreasing conversion per pass. However, a consequence of such obstructions is increased pressure drop through the cell.[92] More recent generations of EMAR cells have incorporated a pin-type flow channel, with rubber dots arranged in a regular pattern. These cells have exhibited significant performance improvements compared to earlier versions, but it is unclear if and how much the flow channel has contributed to this due to concurrent changes to the cell/system design and operating procedure.[87]

In addition to flow channels, optimization of the electrode geometry will also play a role in improving cell performance. Currently, 2D planar electrodes are used in EMAR. However, in many fields, three-dimensional (3D) porous electrodes have been adopted to enhance performance.[93,94,95] Overall, these porous electrode structures have a significantly higher reaction area per volume, which permits cell operation at higher geometric current densities with reduced overpotentials compared to planar electrodes.[96] In modeling the EMAR system, Stern et al. estimated that a cell with porous electrodes could operate with overpotentials > 50% lower than a cell with planar electrodes.[83] When tested, the use of porous copper foam electrodes within the EMAR cell enabled higher Faradaic efficiencies and lower cell resistances, however, performance diminished over a few hours.[90] They believe this failure was due to

bubble formation and entrapment within the electrochemical cell. To the best of our knowledge, no further work using porous electrodes within the EMAR cell has been published to date.

Issues associated with plating and stripping copper have also hindered system feasibility and cell performance. During operation, the current density is not uniformly distributed across the electrode leading to spatially-varying metal deposition on the cathode and stripping from the anode. Accordingly, authors reported sanding or completely replacing both electrodes between experiments.[90, 97] While less of a concern for exploratory studies at the bench-scale, if unaddressed, electrode degradation has the potential to become a significant maintenance challenge during practical implementation. Furthermore, as current density is increased and mass transport limitations emerge, dendritic copper growths can occur during plating. These deposits can become more powder-like as the cell approaches a mass transport controlled regime.[98] In a cell with convective flow, these more loosely-bound deposits may be sheared away from the surface,[99] resulting in a permanent loss of copper electrode mass over time. Additionally, dendritic copper growths from the electrode surface can puncture the membrane/separator and come into contact with the opposite electrode, resulting in an internal short circuit.[86] Early EMAR cell designs incorporated a woven cotton cloth (cheesecloth) between the membrane/separator and solid electrode to provide support and prevent this type of contact.[83, 86] Use of this material, however, significantly increased the ohmic resistance of the cell. Incorporation of a structured flow field (as described above) not only enhanced mass transport, but also better supported the membrane/separator such that supporting cloth was not required to prevent contact between the electrode and membrane/separator. This arrangement also reduced the ohmic resistance of the cell from 0.6 Ω to 0.0289–0.14 Ω, which led to concomitant decreases in estimated energy requirements for CO_2 separation.[78, 86, 87] The membrane/separator itself also introduces ohmic losses, which depend on membrane/separator class (ion-exchange membrane or porous, non-selective separator) and material. While earlier EMAR demonstrations have mostly used porous, non-selective separators, more recent studies have instead reported using anion-exchange membranes. However, there is no indication of whether this has resulted in performance enhancement.[82, 87]

The discussed studies have led to advances in EMAR cell/system design, which have allowed for significant performance improvements. The improved cell platform afforded lower cell overpotentials and thus improved energetics (40–80 kJ/mol CO_2), as well as greater copper loading swings leading to higher regeneration capacities (0.12–0.62 mol CO_2/mol EDA). Despite these advances, cell operation is still limited by relatively low current densities and challenges with copper plating/stripping.

4.4 Computational Insight into Amine/CO_2 Binding.

The strength by which a particular amine binds the CO_2 molecule is a decisive factor governing the efficiency of both thermal swing and EMAR technologies. Amines that exhibit stronger CO_2 binding can enable higher removal rates of CO_2, but may require more energy to release CO_2 and regenerate the solvent. However, the seemingly simple process of formation of a carbamate through the reaction of an amine with CO_2 is more complicated due to intermediate reactions following the initial CO_2 uptake. Computational modeling has provided insight into the stability of possible reaction intermediates and energetic barriers for their interconversion and decomposition.[100-102] Modeling has also been used to understand how substituent effects are correlated with binding energies, basicities, or nucleophilicities of the CO_2-binding centers, and also how hydrogen-bonding can influence these trends. However, not all fundamental aspects of CO_2 absorption by amine functionalities have been resolved. There is now a clear consensus that the reaction is assisted by participation of the solvent (water) molecules, which play a critical role in the stabilization of reaction intermediates, regardless of their chemical nature. The insufficient modeling of the solvent environment has thus led to inconsistencies in the theoretical models, resulting in contrasting conclusions.

In the pioneering works on the MEA-CO_2 binding mechanism, Da Silva and Svendsen[103] and Shim et al.[104] suggested that the carbamate product is formed *via* a single-step, third-order reaction mechanism. The CO_2 molecule is proposed to bind to one MEA molecule and concurrent deprotonation by a second MEA increases its basicity (**Figure 6A**). Alternatively, another base or a solvent molecule can substitute the second MEA molecule in the mechanism. In another study,[105] Da Silva and Svendsen recognized a significant stabilization of both the zwitterionic intermediate and the carbamate by the solvent microenvironment and suggested that a zwitterionic intermediate (initially thought to be a transition-state structure) may be present in the (two-step) mechanism (**Figure 6B**), although it would likely be short-lived.

Arstad et al. proposed another mechanism for MEA-CO_2 binding,[106] in which the carbamic acid is formed from the same zwitterionic intermediate through a proton-relay mechanism. In such a pathway, proton transfer is assisted by a solvent (water) molecule, or an additional amine species (*cf.* **Figure 6C**).

A:

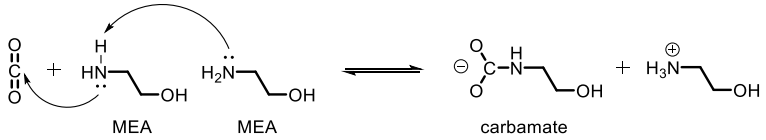

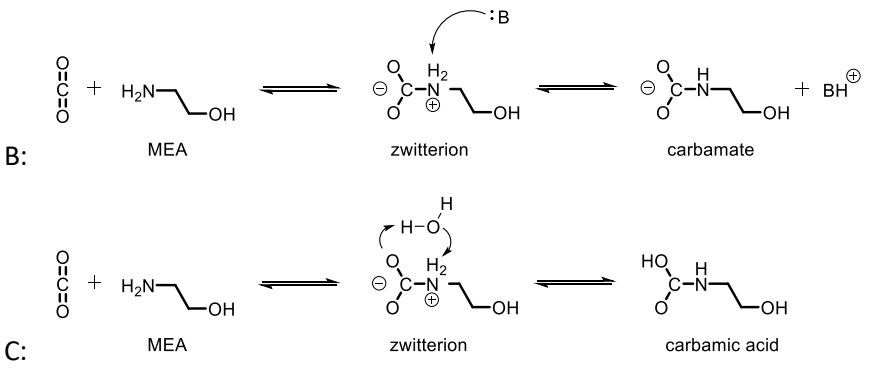

Figure 6. Three suggested reaction mechanisms for CO_2 absorption by MEA: (A) MEA binds one CO_2 molecule and concurrent deprotonation by a second MEA forms a carbamate; (B) MEA binds one CO_2 molecule to form a short-lived zwitterionic intermediate which is followed by deprotonation by another base (e.g., amine) or solvent to form a carbamate; (C) MEA binds one CO_2 molecule to form a short-lived zwitterionic intermediate which is followed by a proton transfer from a solvent (water) or amine molecule to form carbamic acid.

Sumon et al. advocated for the use of a more advanced semi-explicit solvation model to obtain accurate energetics, and they included up to 20 water molecules in a hydrogen-bonded cluster around the solutes.[107] A further improved model included the dynamical behavior of the systems obtained from the molecular dynamics. This approach is significantly more demanding, as the advanced evaluation of the free energies along with the sampling of the solvent configurational space is required. As an example of this approach, both mechanisms in Figures 6a and 6b were re-evaluated by Xie et al.[108] Based on *ab initio* calculations (at the CCSD(T) level of theory) combined with quantum mechanics/molecular mechanics/molecular dynamics simulations (QM/MM/MD), the authors concluded that the two-step reaction mechanism to form a carbamate through a zwitterionic intermediate (**Figure 6B**) is the most likely, contrasting with the 'carbamic-acid' pathway. In accordance with the barrier obtained from the experiment, they observed the rate-limiting step to be associated with the MEA(CO_2) formation at ca. 12 kcal/mol, which was primarily attributed to the breaking of the hydrogen-bonding network around the CO_2 molecule to initiate binding to MEA.

Employing the (DFT-based) *ab initio* molecular dynamic simulations (AIMD), the stability and mutual interconversion of the reaction intermediates along the two-step CO_2 capture process from **Figure 6B** (CO_2 + MEA → zwitterion → carbamate) was also studied.[109-114] More specifically, Han et al. observed rapid deprotonation of the zwitterionic intermediate, forming a stable carbamate species,[109] which was recognized as the principal driving force for CO_2 absorption. Noticeably, the same zwitterion →

carbamate transformation was also supported by the unbiased AIMD,[110] allowing estimation of the zwitterionic intermediate lifetime to be ca. 100 ps.

To some extent, complementary results were later acquired by Guido[110] and by Hwang,[109] which focused on the stability of the zwitterionic intermediate with respect not only to the zwitterion deprotonation (i.e., carbamate formation) but also to CO_2 removal (i.e., MEA regeneration). A delicate balance between the competing pathways was identified in both of the studies, which was deemed to be further complicated by significant temperature and entropic effects that contributed to the free energies from extensive reorganization of the solvent microenvironment. The solvent participation was shown to go far beyond the first solvation shell, providing further evidence of the inadequate use of the continuum (even semi-explicit) solvation models.

The tight balance between zwitterion → carbamate and zwitterion → CO_2 + MEA competition was also acknowledged in investigating CO_2 release from carbamate.[113] Since the calculations revealed that the process is too energetically demanding, the authors made use of the reversibility of the reactions, proposing that CO_2 release is accomplished by *(i)* regeneration of the zwitterionic intermediate by carbamate protonation by MEA(H^+), and *(ii)* CO_2 release from the zwitterionic intermediate (i.e., reverse of the reaction pathway B in **Figure 6**).

Finally, Matsuzaki et al. investigated the mechanism for the formation of the bicarbonate product.[115] Based on the *ab initio* calculations along with the PCM solvation model, they suggested that the formation of the carbamate intermediate (**Figure 6B**) is followed by its protonation in the next step, yielding the carbamic acid. The carbamic acid is then speculated to further undergo an attack by OH^-, releasing the bicarbonate and free MEA.

Other studies – not directly focused on the mechanism of the CO_2-amine interaction – were carried out to screen the additional effects of molecular structure (e.g., amine substitutions), solvent environment, temperature, and other experimental conditions. A few examples include the calculations of various amines' basicities and their correlation with the CO_2 interaction energies (stability of the carbamate intermediate) and/or the reaction kinetics.[105, 116-119] Naturally, the electron-withdrawing groups weakened CO_2 binding efficiency as their basicity decreased, and *vice versa*. In addition, Orestes et al. proposed that higher basicity implies greater stability of the zwitterionic intermediate, and therefore, suggested that highly basic amines (such as guanidines) may provide relatively stable zwitterions with prolonged lifetimes.[116] This greater stability indicates a stronger bond with CO_2 to form the carbamate through hydrogen atom transfer of the hydrogen atom bound to the amino nitrogen. Jhon

et al. tried to evaluate steric effects to explain the contrasting patterns in the nucleophilicity of various amines and their reactivity, but further evaluation is needed to predict better CO_2-amine reactivities.[120]

Finally, Li et al. evaluated the performance of various exchange-correlation functionals for predicting the MEA-CO_2 interaction.[121] The authors observed somewhat inconsistent results on the optimized geometries and the corresponding energies based on the method that was utilized. In particular, the energetic minima seem to differ significantly when the MP2 or DFT optimizations were performed, which raises concerns as to the accuracy of the *ab initio* single-point calculations carried out on top of the DFT optimized geometries. However, it seems that the ωB97XD functional can be recommended for both optimization and energetic purposes.

In summary, the described theoretical studies have focused on understanding the binding mechanism between amines and CO_2. The primary/secondary amines are believed to react with CO_2 molecules to provide carbamate species through the short-lived zwitterionic intermediate. The strength of the amine-CO_2 interaction is regulated by the basicity (nucleophilicity) of the amines that can, in turn, be controlled by the introduction of the electron-donating/withdrawing substituents. Theoretical studies have also indicated the close participation of the solvent (water) molecules, as these species can stabilize the free reactants (by forming a concise hydrogen-bonding network around them) or particular reaction intermediates (such as zwitterionic intermediate or carbamate), or can function as proton relays to accept/donate protons. Therefore, it comes as no surprise that solvent models that treat water molecules explicitly (or semi-explicitly) exhibit more reliable results than simple continuum-based approaches. On the other hand, the mechanism of CO_2 release is still relatively underexplored, as several contrasting reaction pathways have been suggested.

5. Redox-Active Capture Molecules.

5.1 Introduction.

Another popular approach to eCCC is the use of redox-active capture molecules, or redox carriers, that directly bind and release CO_2 upon oxidation or reduction (i.e., direct eCCC methods). Scheme 4 illustrates a generalized direct eCCC cycle featuring a redox carrier.[122] In the cycle, the molecule in the resting state (R) is reduced to form the active state carrier species (R^{n-}), where n is the number of electrons transferred. The reduced species has a high affinity for CO_2 ($K_{1(R^{n-})}$), which allows for capture from a dilute inlet stream to form the CO_2-bound adduct, $\mathrm{R}(\mathrm{CO}_2)_q^{n-}$. Here, q represents the number of CO_2 molecules that bind to each capture molecule. Release is triggered by the oxidation of $\mathrm{R}(\mathrm{CO}_2)_q^{n-}$ to form $\mathrm{R}(\mathrm{CO}_2)_q$, which has a much lower affinity for CO_2 ($K_{2(\mathrm{R})}$), resulting in liberation of CO_2 to reform

the resting-state carrier (R) to complete the cycle. This approach takes advantage of the difference between the binding affinity of the oxidized ($K_{2(\mathrm{R})}$) and reduced ($K_{1(R^{n-})}$) states of the carrier (R and R^{n-}, respectively).

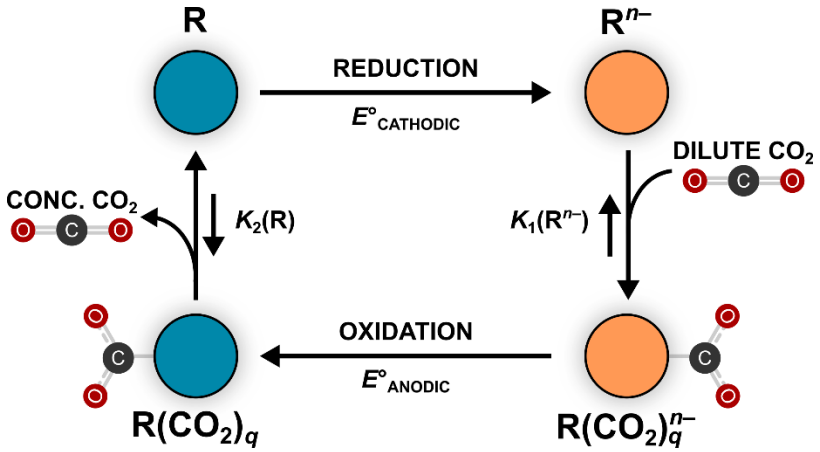

Scheme 4. Redox-active capture molecules for electrochemically-mediated CO_2 separation, adapted from Ref. 41.

DuBois and coworkers were the first to publish the use of redox-active capture molecules for eCCC applications. Several classes of redox-active capture molecules were assessed using spectroscopic, voltammetric, and controlled potential electrolysis approaches to determine both the electrochemical reversibility of CO_2 binding and the CO_2 equilibrium constants of the oxidized and reduced forms.[123,124] In these works, they outline desirable molecular properties of efficient CO_2 capture molecules. They propose that a capture molecule for direct eCCC must have a site capable of CO_2 binding and must also be able to undergo chemically reversible oxidation and reduction in the presence and absence of CO_2. Regarding these two points, they identified the importance of proximity of the redox center to the CO_2 binding site. Shorter distances between the two sites resulted in larger changes in the binding affinity between oxidized and reduced states of the capture molecule. This is important because the difference in CO_2 binding affinity between the oxidized and reduced forms must be sufficiently large to enable sufficient CO_2 capture from a given feed gas. One metric that can be utilized to evaluate if sufficient CO_2 is captured from the feed gas is the Faradaic efficiency, or the moles of CO_2 separated per mole of electron transferred. Assuming complete activation/deactivation of a redox-active capture molecule (with total concentration $[\mathrm{R}]_\mathrm{T}$), the upper bound on η_{faradaic} for a redox-active carrier / solvent system can be determined as follows:

$$\eta_{\mathrm{faradaic}} = \frac{q}{n}\left(\frac{K_{1(\mathrm{R}^{2-})}(K_\mathrm{H}P_\mathrm{i})^q}{1+K_{1(\mathrm{R}^{2-})}(K_\mathrm{H}P_\mathrm{i})^q} - \frac{K_{2(\mathrm{R})}(K_\mathrm{H}P_0)^q}{1+K_{2(\mathrm{R})}(K_\mathrm{H}P_0)^q}\right) - \frac{K_\mathrm{H}}{n[\mathrm{R}]_\mathrm{T}}(P_0 - P_\mathrm{i}) \qquad \text{Eq. 9}$$

where K_{H} is the Henry's law constant for CO_2 in the solvent of choice, P_{i} is the initial CO_2 partial pressure before separation, and P_{f} is the final CO_2 partial pressure after separation and recovery (typically 1 atm). This expression for the Faradaic efficiency upper bound aligns with several previous works.[124, 125, 126] Considering an example system with a 10% CO_2 stream (typical concentration from a coal-fired power plant flue gas)[23, 28] and the following constant parameters ($[\mathrm{R}]_{\mathrm{T}}$ = 1 M, K_{H} = 0.175 M/atm, $K_{2(\mathrm{R})} \ll 1$, q = 1), a $K_{1(\mathrm{R}^{n-})}$ value of at least 6.3 x 10^2 is required to obtain ≥ 90% of the maximum Faradaic efficiency predicted with eq. 9. Using the same equation, a $K_{1(\mathrm{R}^{n-})}$ value of at least 1.6 x 10^5 is necessary to capture from atmospheric CO_2 sources (P_{i} = 410 ppm) with the same efficiency.

In addition to impacting the Faradaic efficiency, binding coefficients can also influence system energy requirements due to their direct relation to the difference in standard potentials for the binding and release steps ($\Delta E = E^{\circ}_{\text{cathodic}} - E^{\circ}_{\text{anodic}}$). More specifically, the ratio between the activated and deactivated capture molecule binding affinities, i.e., $K_{1(\mathrm{R}^{n-})}/\,K_{2(\mathrm{R})}$, is intrinsically proportional to ΔE according to eq. 10.

$$-RT \ln\left(\frac{K_{1(\mathrm{R}^{n-})}}{K_{2(\mathrm{R})}}\right) = nF(\Delta E) \qquad \text{Eq. 10}$$

Therefore, a higher binding affinity ratio, $K_{1(\mathrm{R}^{n-})}/\,K_{2(\mathrm{R})}$, will lead to higher cell voltages and thus greater energy requirements. To further assess this tradeoff between system energy requirements and Faradaic efficiency, Clarke et al. defined a combined efficiency metric to highlight molecular properties (such as $K_{1(\mathrm{R}^{n-})}$) that may be effective to adequately balance this tradeoff.[126] Their work also explores how these effective properties are dependent upon other system properties, such as system configuration.

Beyond having adequate CO_2 binding affinities while maintaining a minimal potential difference between binding and release steps, additional desirable characteristics of capture molecules include: rapid electron transfer kinetics, high solubility, stability of the carrier species towards other compounds present in a given feed gas composition (e.g., oxygen, water vapor), among others.[42, 43, 125] Overall, several different classes of molecules have been identified and assessed as capture molecule candidates. Quinones are the most studied group of molecules, [110, 113, 127-131] but other redox-active capture species have been assessed as well, including transition-metal complexes,[132] bipyridines,[133-135] and thiols.[136] In the following sections, several demonstrations involving different capture molecules and solvents will be discussed. These demonstrations include primarily cyclic voltammetry and bulk electrolysis experiments to assess CO_2 binding/release capabilities, as well as a few engineered flow-cell systems.

5.2 Mechanistic Insights and Demonstrations.

5.2.1 Quinones.

In addition to acting as reversible PCET pH-mediators (as discussed in Section 3), *ortho*- and *para*-benzoquinones can bind CO_2 directly under aprotic conditions. CO_2 reacts with reduced quinones at one or more anionic oxygen atoms via an ECEC or EEC mechanism.[128] An ECEC mechanism may be desirable because the quinone captures two CO_2 molecules, increasing the sorbent capacity. Additionally, capturing two CO_2 molecules per two electron transfers theoretically allows for Faradaic efficiencies of 100%. ECEC or EEC mechanisms depend on whether CO_2 molecules bind to the reduced species in its radical anion (Q_{RA}) and/or dianion (Q_{DA}) forms (Scheme 5).[127-129] In general, quinones have displayed a wide range of affinity for CO_2; reported CO_2 binding constants for quinone dianions ($K_{\mathrm{CO_2(DA)}}$) have been reported between ca. 10 – 10^{20}[20,124, 128, 137-141] which is summarized in Table 1. Numerous quinones also bind CO_2 in their radical anion state (Q_{RA}). However to date, $K_{\mathrm{CO_2(RA)}}$ values have only been reported for 9,10-phenanthrenequinone and 2,6-di-*tert*-butyl-1,4-benzoquinone.[124, 137] The binding constants for both radical anions ($K_{\mathrm{CO_2(RA)}}$) were several orders of magnitude smaller than the corresponding values for the dianions ($K_{\mathrm{CO_2(DA)}}$). Although no other values of $K_{\mathrm{CO_2(RA)}}$ have been quantitatively determined, cyclic voltammetry suggests that $K_{\mathrm{CO_2(RA)}}$ is always much smaller than $K_{\mathrm{CO_2(DA)}}$,[124, 128, 129, 137, 138, 140] likely due to increased nucleophilicity of the oxygen atoms in the dianion. The specific value for $K_{\mathrm{CO_2(RA)}}$, which represents the thermodynamic favorability of CO_2 binding to a quinone radical anion species, causes the disparity in reported mechanisms (EEC or ECEC). A complication to this assessment, however, is if disproportionation of two Q_{RA} molecules transpires to create Q and Q_{DA}, which then reacts with CO_2; this may result in inflated values for $K_{\mathrm{CO_2(RA)}}$ and falsely suggest an ECEC mechanism if not properly considered.[124, 142, 143]

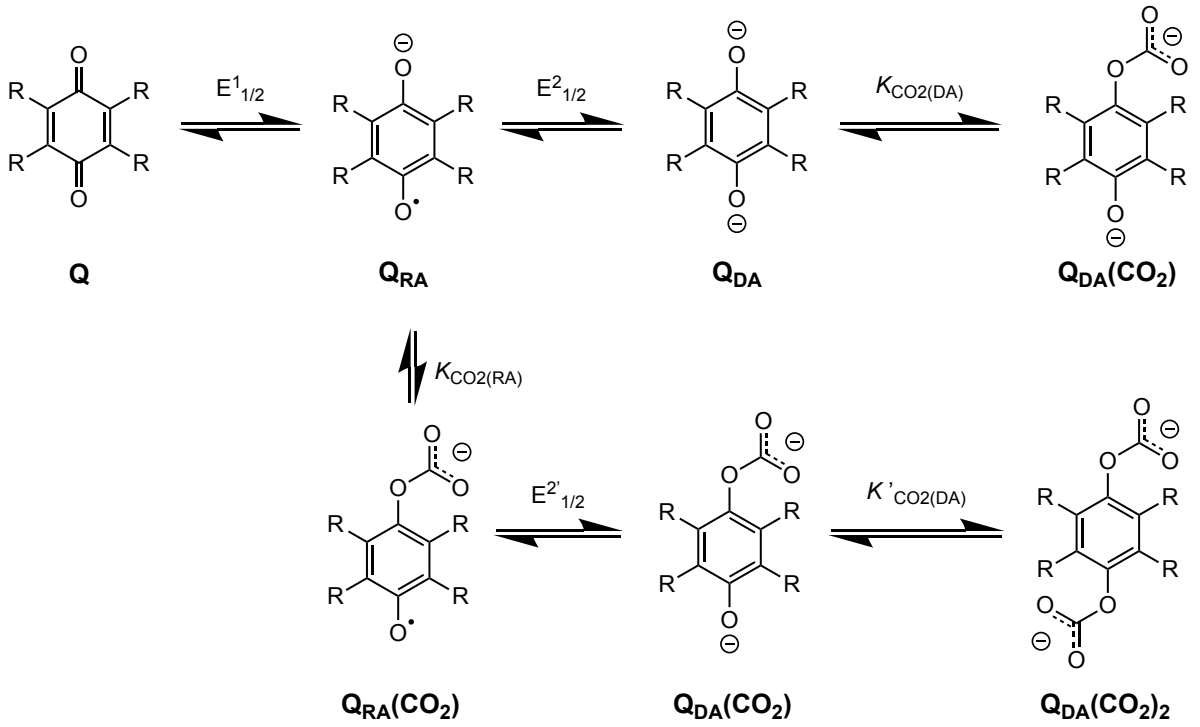

Scheme 5. Direct electrochemical capture by quinones by EEC mechanism (top) and ECEC mechanism (bottom).

Table 1. Reported reduction potentials for various quinone radical anion / dianion redox pairs ($E^2_{1/2}$) and associated CO_2 binding constants of the dianion species ($K_{CO2(DA)}$).

Quinone	Solvent	$E^2_{1/2(N2)}$[a]	$E^2_{1/2(CO2)}$[a]	$\Delta E_{1/2}$[b]	Log($K_{CO2(DA)}$)	Ref.
Tetrachloro-1,4-benzoquinone	DMF	–0.72	N/A	N/A	3.8	120
2,6-di-tert-butyl-1,4-benzoquinone	DMF	–1.46	N/A	N/A	15.0	120
9,10-phenanthrenequinone	DMF	–1.19	N/A	N/A	11.8	120
2,3-dicyano-1,4-benzoquinone[c]	DMF	–0.47	N/A	N/A	3.8	121
tetrafluoro-1,4-benzoquinone	DMF	–0.80	–0.50	0.30	4.3	135
tetrabromo-1,4-benzoquinone	DMF	–0.88	N/A	N/A	3.3	136
2,3-dichloro-1,4-naphthoquinone	DMF	–1.21	N/A	N/A	5.7	136
2,5-bis(dimethylamino)-3,6-difluoro-1,4-benzoquinone	DMF	–1.47	N/A	N/A	11.6	136
1,4-benzoquinone[c]	DMSO	–1.05	0.00	1.05	16.9[e]	137
anthraquinone (AQ)	DMSO	–1.40	–0.65	0.75	11.8[e]	137
duroquinone	DMSO	–1.55	–0.33	1.22	19.9[e]	137
naphthoquinone (NQ)	DMSO	–1.25	–0.40	0.85	13.5[e]	137
2,6-dimethyl-1,4-benzoquinone	DMSO	–1.40	–0.23	1.17	19.0[e]	137

2, 6- dichloro- 1, 4-benzoquinone	MeCN	–0.94	–0.60	0.34	6.0	125
2- chloro- 1, 4-benzoquinone	MeCN	–1.07	–0.58	0.49	10.0	125
tetrafluoro-1, 4-benzoquinone	MeCN	–0.80	–0.62	0.18	3.8	125
tetrachloro-1,4-benzoquinone	MeCN	–0.74	–0.63	0.11	2.5	125
5-hydroxy- NQ[d,]**	MeCN	–0.94	–0.71	0.23	3.3	125
1, 8- dihydroxy- AQ[d,]**	MeCN	–1.20	–0.94	0.26	5.4	125
1, 2- dihydroxy- AQ[d,]**	MeCN	–1.29	–1.08	0.21	4.6	125
5, 8- dihydroxy- NQ[d,]**	MeCN	–0.98	–0.91	0.07	2.1	125
anthraquinone	MeCN	–1.56	–0.62	0.46	9.0	138
1-hydroxy-AQ	MeCN	–1.30	–1.18	0.20	5.1	138
1,4-dihydroxy-AQ	MeCN	–1.15	–1.14	0.01	1.1	138
1-amino-AQ	MeCN	–1.58	N/A	N/A	8.3	138
1,4-diamino-AQ	MeCN	–1.63	N/A	N/A	9.7	138
1-amino-4-hydroxy-AQ	MeCN	–1.41	–1.20	0.21	4.8	138
2,3-dicyano-1,4-naphthoquinone	MeCN	–0.62	N/A	N/A	1.7	136
2,5-bis(dimethylamino)-1,4-benozquinone	MeCN	–1.23	N/A	N/A	12.1	136
tetra(dimethylamino)-1,4-benzoquinone	MeCN	–1.68	N/A	N/A	11.6	136
tetramethylester-1,4-benzoquinone	$CHCl_3$	–0.65	N/A	N/A	2.5	136

[a]Potentials are reported as V vs. SCE. Potentials recorded in MeCN were converted to SCE using Ref. [144]
[b] Reported in units of volts and equal to the shift in half-wave potential in the presence and absence of CO_2 ($\mathbf{\Delta E_{1/2}} = E^{o\prime} - E_{1/2}$ in eq. 11).
[c]Undergoes Kolbe-Schmidt reaction with CO_2 as a decomposition pathway.
[d]Features intramolecular hydrogen-bonding interactions.
[e] Calculated using eq. 11 from reported reduction potentials under N_2 and CO_2 atmosphere.

Among the multiple classes of redox-active molecules first considered by DuBois and coworkers, quinones were the most promising. [137] A wide variety of quinone candidates were screened in acetonitrile (MeCN) and dimethylformamide (DMF) using both cyclic voltammetry and bulk electrolysis techniques. Of the large number investigated, only five showed reversible CO_2 binding and release with sufficient CO_2 binding affinities: 2,6-di-*tert*-butyl-1,4-benzoquinone (DtBBQ), 9,10-phenanthrenequinone (PAQ), tetrachloro-1,4-benzoquinone (TCQ), 2,3-dicyano-1,4-benzoquinone, and 2,3-dicyano-5,6-dichloro-1,4-benzoquinone (DDQ). Reduction potentials and values of $K_{\mathrm{CO_2(DA)}}$ (and some values of $K_{\mathrm{CO_2(RA)}}$) were reported for each of the five quinones, however little mechanistic information was determined beyond the number of CO_2 molecules bound per quinone dianion.

In 1989, Mizen and Wrighton reported the first mechanistic study of CO_2 binding to quinone dianions.[127] Chemical reduction of PAQ by one or two electrons with cobaltocene or sodium metal (to form $PAQ^{\bullet-}$ or PAQ^{2-}, respectively), followed by addition of CO_2 resulted in the formation of a new species.

This species featured a ^{13}C NMR peak between 156-158 ppm in CD_3CN or DMSO-d_6, suggesting formation of an alkyl carbonate. Infrared spectroscopy further confirmed this assessment, exhibiting carbonyl stretches at 1646 and 1686 cm^{-1} when cobaltocene was used as the reductant. Spectroelectrochemical infrared (SEC-IR) spectroscopy indicates the formation of a single carbonyl stretch at 1646 cm^{-1} upon reduction of PAQ to PAQ^{2-}. The stretch observed at 1686 cm^{-1} was attributed to interactions with cobaltocenium cation, which is more likely to interact and stabilize the CO_2 adduct than the tetrabutylammonium cations present in SEC-IR studies. When the same experiments were repeated in the absence of CO_2, the ^{13}C NMR and IR signals were not observed, which indicated CO_2 binding occurs at one or both anionic oxygen atoms upon reduction of PAQ to PAQ^{2-}. With this information, along with the experimentally determined 2:1 ratio of CO_2:PAQ^{2-}, Mizen and Wrighton proposed an ECEC mechanism for the reaction, whereby two molecules of CO_2 are bound through the two oxygen atoms of PAQ^{2-}.

Shortly thereafter, Ogura and coworkers reported a mechanistic study with several other quinones and CO_2 in MeCN.[128] This study expanded upon the work of Mizen and Wrighton by including 11 different quinones of varying electron density. Like PAQ, the quinones with more nucleophilic oxygen atoms bind two molecules of CO_2 via an ECEC mechanism. In contrast, the less electron dense quinones did not bind CO_2 in the radical anionic state and thus undergo an EEC to bind one molecule of CO_2 upon reduction to the dianion. Interestingly, the authors observed that there appeared to be a specific threshold potential for the first reduction (to form the radical anion) where the quinones switched between EEC and ECEC mechanisms. The proposed ECEC mechanism for 1,4-anthraquinone (AQ), 1,4-napthoquinone (NQ), duroquinone (DQ), and 2,6-dimethylbenzoquinone (DMQ) in MeCN by Ogura and coworkers contrasts with the mechanism previously reported in dimethylsulfoxide by Simpson and Durand.[140] Simpson and Durand proposed an ECE mechanism for each of these quinones based on cyclic voltammetry; however the authors did not determine how many CO_2 molecules were bound to the reduced quinone species. Due to the difficulty of differentiating ECE and ECEC mechanisms by cyclic voltammetry and without knowledge of either reaction stoichiometry or products formed,[145] it is likely that the mechanism was incorrectly assigned and is in fact ECEC for these quinones. In more recent work, naphthoquinones have been determined to undergo ECEC or EEC mechanisms in ionic liquid solvents, similar to what has been previously observed in aprotic organic solvents.[129]

To study the redox behavior and the reactivity toward CO_2 capture of *p*-benzoquinone (BQ) and tetrafluoro-*p*-benzoquinone (TFBQ), Namazian et al. employed both experiments (cyclic voltammetry) and theory (ab initio calculations with the G3MP2//B3LYP composite method with the CPCM solvation model).[138] Their cyclic voltammetry results in DMF solvent indicated that BQ is likely to capture CO_2 after

the first reduction to BQ semiquinone ($BQ^{\bullet-}$), whereas the TFBQ was proposed to react with CO_2 only after the two-electron reduction ($TFBQ^{2-}$) is accomplished (note that this corresponds to the ECE and EEC mechanisms for BQ and TFBQ, respectively). In the article, the lower reactivity of the TFBQ semiquinone was explained based on the lower nucleophilicity of the quinone's oxygen atoms due to the presence of the electron-withdrawing fluorine atoms. The calculation of the lower charge on the oxygen atoms in $TFBQ^{\bullet-}$ was performed as a confirmation. The BQ and TFBQ were also compared in the regioselectivity of CO_2 binding. Both theory and experimental work indicate that $TFBQ^{2-}$ binds CO_2 at the oxygen atom, forming a carbonate product (note that the carbonate was calculated to be favored by ~ 88 kJ/mol over the carboxylate). Comparatively, theory predicts that BQ prefers carboxylate (carbon-bound CO_2) over the carbonate product by ~ 10 kJ/mol. However, these findings conflict with previous experimental observations, and they speculated that this difference may be due to kinetics, as the formation of the carbonate product may be a faster reaction than the that to form the more stable carboxylate product. While formation of a carboxylate versus a carbonate does not affect the overall mechanism (i.e., EEC or ECE) in theory, it is unclear if and how the resulting product would impact overall performance of a redox active capture molecule. Fan et al. revisited the BQ reactivity by comparing the properties of the most stable carboxylate species obtained from the calculations with the experimental infrared absorption, and notably, the authors' findings were in agreement.[146]

Naphthoquinones undergo ECEC or EEC mechanisms in ionic liquid solvents, similar to what has been observed in aprotic organic solvents.[129] Jin and coworkers used a spectroelectrochemical approach to elucidate the mechanism and site of binding for CO_2 capture with NQ, 2-chloro-1,4-napthoquinone (CNQ), and 2,3-dichloro-1, 4-napthoquinone (DCNQ). Upon two electron reductions of NQ to the dianion (NQ^{2-}) under CO_2, a carbonyl stretch is observed at 1634 cm^{-1} via spectroelectrochemical infrared spectroscopy (SEC-IR). The IR band is consistent with a carbonate species and is not present when the experiment is repeated in an inert N_2 atmosphere. This result suggests that CO_2 binds to NQ^{2-} through the anionic oxygen atoms, similar to what was previously observed with PAQ^{2-} in MeCN.[127] Using cyclic voltabsorptometry (CVA) and derivative cyclic voltabsorptometry (DCVA), the authors concluded that reaction of CO_2 with NQ follows an ECEC mechanism using. Monitoring the IR spectrum during CVA and DCVA experiments, it was observed that the CO_2 binds to the radical anion ($NQ^{\bullet-}$) prior to being reduced to the dianion, where it could then bind a second molecule of CO_2. The overall reaction stoichiometry of NQ with CO_2 was further confirmed using a similar method used by Ogura and coworkers.[128] When the solution was oxidized, the carbonate stretch at 1634 cm^{-1} disappeared, with the growth of a peak at 1671 cm^{-1} corresponding to NQ. This pattern was observed across multiple consecutive scans, indicating that binding and release is

reversible. When these experiments were repeated for CNQ and DCNQ, similar results were observed; however, both quinones only bind one molecule of CO_2 through a proposed EEC mechanism.

While thermodynamic data exists for CO_2 binding with various quinone dianion species and some anion species, much less kinetic information has been reported. Yet, CO_2 reaction kinetics will play an important role in overall system performance as they will influence the rate of CO_2 binding/release and, consequently, the design and performance of associated process units (e.g., absorption column). In early work, Wrighton and Dubois investigated the kinetics of binding between quinones (PAQ and DTBBQ, respectively) and CO_2 following reduction. Using chronoamperometric techniques, they obtained second order rate constants of 96 and 19.1 $M^{-1}s^{-1}$ for $PAQ^{\bullet-}$ in MeCN and $DtBBQ^{\bullet-}$ in DMF, respectively.[124, 127] Durand and coworkers performed a kinetic investigation of CO_2 binding with a series of quinones in a single solvent.[140] Using rotating disk voltammetric methods, the second order rate constants for five quinones were determined, ranging between 46 to 350 $M^{-1}s^{-1}$ in DMSO. The second order rate constants were derived using digital simulations based on data obtained under pseudo-first order conditions, instead of by varying the concentrations of CO_2 as was done in prior studies. Results from the five quinones indicate that there may be a relationship between the first (more oxidative) reduction potential and CO_2 binding rate constant, such that more negative reduction potentials (more nucleophilic quinones) correspond with faster binding. However, relatively large errors in the rate constants and the small data set prevents analysis of any observed trends. While it is currently unclear what rate constant values will be required or optimal, there are indications for how rate constants could impact CO_2 binding selectivity. From the limited data reported for quinone CO_2 reactivity, protonation is confirmed to be kinetically favored.[140, 143] For example, protonation of anthraquinone has been observed to be twice as fast as CO_2 binding in DMSO.[140] If an electrochemical separation process requires CO_2 removal from a mixture with high water vapor concentrations, relatively slow CO_2 binding kinetics (as compared to protonation) could significantly reduce capture molecule effectiveness. Thus, careful matching of solvent and quinone pK_a values and/or preclusion of acidic proton sources are necessary to prevent kinetic inhibition of eCCC due to protonation.

In addition to these mechanistic studies, quinones have also been cycled over longer time scales using controlled potential electrolysis or other electrochemical cells to quantitatively demonstrate CO_2 capture and release. Scovazzo et al. first reported a successful proof-of-concept CO_2 capture-release system for direct eCCC, which used solutions of DtBBQ in either propylene carbonate or 1-butyl-3-methylimidazolium hexaflurophosphate ionic liquid ([bmim][PF_6]).[125] Using a closed-system bulk electrolysis set-up, the authors demonstrated that direct eCCC from very dilute (< 1%) inlet streams was plausible and that the

overall CO_2 concentration could be increased to near 100% upon oxidation in a single pass. Using 30 mL of the propylene carbonate solution (0.30 M DtBBQ and 0.75 M tetrabutylammonium tetrafluoroborate supporting electrolyte), 120 mL of pure CO_2 was captured and then released from an incoming 0.5% CO_2 inlet stream. Successful capture, release, and concentration was also performed using [bmim][PF_6] as the solvent and electrolyte. However, the low concentration of DtBBQ compared to the solubility of CO_2 in [bmim][PF_6] (0.05 M versus 0.08 M/atm, respectively) resulted in a less impressive concentration swing, which ranged between 7% to 33% initial and final concentrations. In the two demonstrations, 0.427 and 0.454 moles of CO_2 were released per mole of electron in PC and [bmim][PF_6], respectively, resulting in Faradaic efficiencies of ~43% and ~45%. These Faradaic efficiencies compare well to the maximum Faradaic efficiency of 50% for DtBBQ, as it requires two-electron processes for binding and release, but only one molecule of CO_2 is bound to the dianion. The estimated energetic efficiency of the system is unclear, as no electrode potential difference between the capture and release steps was reported. However, typical bulk electrolysis cells (often referred to as "H-cells"), as such, are non-optimized for high performance operation, and thus, any reported energetic efficiency would likely not be representative of this system's potential.

Hatton and coworkers developed a more engineered cell architecture by using polymeric quinone-based electrodes for eCCC processes (**Figure 7**).[147] Their approach, coined "electro-swing reactive adsorption" (ESA), uses a carbon fiber cathode coated in a suspension of carbon nanotubes (CNTs) and a polymeric anthraquinone (p-AQ) that adsorbs CO_2 directly to the electrode surface upon reduction. To complete the cell, a carbon fiber anode coated in CNT and polyvinyl ferrocene was used. In their first demonstration, the ionic liquid 1-butyl-3-methylimidazolium bis(trifluorosulfonyl)imide ([bmim][Tf_2N]) served as both the solvent and supporting electrolyte. The Faradaic efficiency of the system was 90% based on cycling experiments performed in a sealed container under 100% CO_2 atmosphere. In this demonstration, the cell potential was controlled and switched between -1.3 and 0.5 V while the headspace pressure was monitored to track CO_2 uptake and release by the p-AQ electrode. In addition to sealed cell measurements, an open cell setup was used where a dilute CO_2 stream was passed through an adsorption bed composed of multiple cells. In this setup, the p-AQ electrodes performed quantitative capture from 10% CO_2 inlet streams, with over 80% capture was observed with inlet stream concentrations as low as 0.6%. Additionally, the system was quite robust, with only ~30% degradation after 7000 capture/release cycles. Based on the applied potential difference and Faradaic efficiency (90%), the reported system energy requirements were 90 kJ/mol CO_2 for CO_2 removal and recovery from a 10%

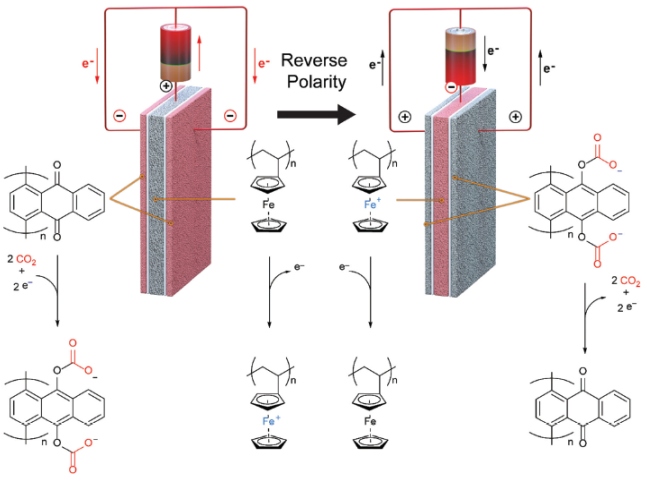

Figure 7. Faradaic electro-swing system with a polymeric anthraquinone electrodes for direct eCCC developed by Voskian and Hatton. Figure used from ref. 144 under the CC BY 3.0 license.

concentration. Based on the reported values, the experimental energetic efficiency of the system is estimated to be ca. 6% (given that a 10% to 100% swing for a case of "skimming" requires 5.7 kJ/mol CO_2). The authors also hypothesize that after several cycles, Δ*E* can be dropped to 500 mV where ~60% of the quinone species are activated for capture. Although it was never evaluated experimentally, dropping Δ*E* to 500 mV is estimated to lower the energetic requirement to ~43 kJ/mol CO_2 (~13% energy efficiency).

More recently, Hatton and coworkers have used their p-AQ electrodes with "water-in-salt" electrolyte mixtures in place of ionic liquids.[148] Large concentrations of lithium bis(trifluoromethylsufonyl)imide (LiTFSI) in water results in a significant extension of the electrochemical window, such that p-AQ could be reduced and oxidized while minimizing solvent or electrolyte side reactions. Due to the reduced concentration of "free-state" water present in 20m LiTFSI at pH 4, protonation of the reduced p-AQ species was suppressed (where m is molality). Due to high supporting salt concentrations, this reactivity runs counter to what has been observed with other quinones in aqueous media[74, 75] as well as what was observed with p-AQ electrodes in 1m NH_4NO_3 at the same pH. Limited proton availability also results in a more anodic potential for the oxygen reduction reaction, decreasing the sensitivity of p-AQ to O_2. Additionally, unlike other reported examples of quinones in the presence of alkali metals,[149-154] the reduction potential of p-AQ does not shift anodically with increasing concentration of LiTFSI (from 1 to 20m) under an inert N_2 atmosphere. When CO_2 was introduced, the reduction peak did shift anodically, indicating the formation of the CO_2 adduct, quinone bis(carbonate), which is oxidized at more positive potentials than the p-AQ dianion. Increasing concentrations of LiTFSI under CO_2 resulted in increased separation between the reduction and oxidation potentials, which was attributed to stabilization of p-AQ CO_2 adducts by LiTFSI, as confirmed by DFT.[147] Using their electro-swing operation strategy with a custom "zero-gap" flow cell, CO_2 binding and release cycles were performed at currents up to 2 mA cm^{-2} (2 A g^{-1}). While operating under constant current conditions of 0.5 mA cm^{-2}, the authors report an energetic

requirement of ~56 kJ/mol CO_2 for their system in 20m LiTFSI, an improvement over the demonstration in [bmim][PF_6], as described above. Based on the reported energy requirement for capture from an initial CO_2 concentration of 15%, an estimated overall efficiency of at least ~8% is calculated (given that a 15-100% swing requires a minimum of 4.7 kJ/mol CO_2 for the case of "skimming"). The system displayed the same excellent stability that was previously observed in [bmim][PF_6], while also operating in the presence of oxygen. A faradaic efficiency of over 95% was averaged over 75 cycles in 20m LiTFSI under a gas composition of 15:3:82 CO_2:O_2:N_2. Hatton and coworkers continued to add alkali metals, albeit at lower concentrations (1 M NaTFSI), in their work with 2,3-Di-(2-(2-methoxyethoxy)ethoxy)-1,4-naphthoquinone, also referred to as a liquid quinone.{Diederichsen, 2022 #1289} Here, they demonstrated capture from a 15% CO_2 mixture (85% N_2), operating at ca. 70% Faradaic efficiency (defined as CO_2 capacity utilization efficiency) while maintaining relatively low levels of efficiency decay over 10 cycles. When 5% O_2 was added to the mixture, efficiency losses were increased, and thus the authors emphasized that understanding O_2 reduction rates in this system will be a focus of future work. They also developed a continuous flow lab-scale test system and demonstrated CO_2 capture and release from a pure CO_2 stream (due to limitations on quinone conversion) and estimated that cell energy requirements could be in the range of 35–220 kJ/mol CO_2.

Recently, to address the observed instability of quinone carriers in the presence of O_2, Zito et al. investigated the validity of the proposed linear relationship between the second reduction potential and CO_2 binding constant of quinones.[139] In their work, they synthesized and tested the ability of seven new quinones to capture CO_2 in their dianion states. The measured $K_{\mathrm{CO_2(DA)}}$ were in the range of ca. 50–10^{12} and followed the trend of decreasing reduction potentials with increasing $K_{\mathrm{CO_2(DA)}}$. The experimental investigation was complemented by large-scale DFT calculations oriented on understanding how the substituent effects on the quinone scaffold influence the key thermodynamic properties (such as reduction potentials and CO_2 binding constants) through steric and electronic effects. Overall, Zito et al. found that the linear trend holds relatively well over a large range of reduction potentials, suggesting that additional secondary interactions might be required to shift the reduction potentials more positive than the O_2 reduction reaction. This could be achieved, e.g., via auxiliary binding charged groups or hydrogen bond donors.

The effects of hydrogen bond donors was probed by Barlow et al. who demonstrated that use such additives indeed shifts the reduction potential of the redox-active capture molecule to more positive potentials.[155] Different alcohols were added to tetrachloroquinone (TCQ) in DMF to study the effect of these hydrogen-bond donors on the reduction potential and the CO_2 binding affinity. Although all alcohol

additives resulted in a positive shift of the reduction potential, stronger hydrogen-bonding interactions inhibited CO_2 binding, leading to smaller CO_2 binding affinities, while moderate interactions resulted in larger CO_2 binding affinities. Ethanol was identified as a hydrogen-bond donor that did not have deleterious effects on the CO_2 binding affinity but enabled a favorable shift in the reduction potential to values greater than that of O_2 reduction. TCQ was tested via controlled potential electrolysis with the presence and absence of ethanol in the electrolyte mixture, where the reduced form of TCQ (TCQ^{2-}) was oxidized and re-reduced in the presence of a simulated flue gas mixture (87:10:3 N_2:CO_2:O_2). With ethanol as an additive, Barlow et al. showed improvements in the extent of electrochemical CO_2 capture and concentration from flue gas concentrations in the presence of O_2. More specifically, with the addition of ethanol, the estimated Faradaic efficiencies during both oxidation/release and reduction/recapture steps were improved from 84% to 95% and 27% to 73%, respectively. The TCQ/ethanol pair was not tested over multiple cycles, so long term stability of this specific chemistry is unclear. However, this work demonstrates that hydrogen-bond donors can be added to an electrolyte to anodically shift the reduction potentials of the quinone (or another redox active capture agent) and improve O_2 stability.

5.2.2 Transition Metals.

Redox-active transition metal (TM) centers paired with specific ligands can also serve as CO_2 capture agents in direct eCCC systems. DuBois and coworkers suggested that TM complexes with ligands that contain a CO_2 binding site (i.e., a nucleophilic nitrogen or oxygen) could achieve CO_2 pumping.[124] The metal center as the active redox site would alter the electron density of the compound and thus the CO_2 binding affinity. Their study found that the distance between the redox metal center to CO_2 binding site significantly impacts the electronic communication of the compound. The assayed compounds contained one, two, or five atoms separating the binding site to the redox active metal center of Co, Fe, or Ru. CO_2 capture activity was only observed in the Co^{3+} cyclopentadienyl indenyl complex with a one-atom separation of metal from the binding site.

A few binuclear TM complexes explored in other works were demonstrated to trap the CO_2 dissolved in aqueous media as a bound carbonate ion.[156-159] In these, specific bridging ligands orient two metals (Zn, Co, Ni, or Cu) to issue strong carbonate binding interactions. However, studies examining the electrochemical behavior of these compounds and their application to reversibly pumping CO_2 are limited.

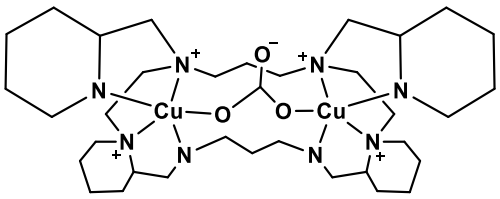

Figure 8. Carbonate adduct, $[Cu_2(tpmc)(\mu\text{-}CO_3)]^{2+}$ formed from $[Cu_2(tpmc)(\mu\text{-}OH)]^{3+}$.

DuBois and coworkers examined binuclear Ni and Cu complexes with varied bridging ligands for the reversible capture and release of bicarbonate, and found that more flexible ligands resulted in enhanced binding.[132, 159] However, the reduction potentials of the nickel complexes were too negative for electrochemical pumping. Of the copper complexes surveyed, the $[Cu_2(tpmc)(\mu\text{-}OH)]^{3+}$ complex (tpmc = bridging *N,N′,N′′,N′′′*-tetrakis(2-pyridylmethyl)-1,4,8,11-tetraazacyclotetradecane ligand), demonstrated a viable reduction potential for CO_2 pumping and successful electrochemical CO_2 capture and concentration from 10% to 75% (**Figure 8**) in the presence of oxygen. Cycling resulted in partial precipitation of the Cu^+ complex, an outcome which could potentially be improved upon with variation of supporting electrolytes or ligand. Contrary to typical increased CO_2 binding affinity upon reduction, these systems bind carbonate upon *oxidation*, and *reduction* results in CO_2 release.

5.2.3 Bipyridines.

Bipyridines also become more nucleophilic upon reduction, making them suitable candidates as CO_2 capture redox carriers. A study by Hitoshi et al. described the reversible capture and release of CO_2 by *N*-propyl-4,4'-bipyridinium ($Prbipy^+$).[133] More recently, Buttry and coworkers explored the reactivity of the related *N*-methyl-4,4'-bipyridinium ($Mebipy^+$) with experimental data and theoretical calculations.[134] The electrochemical behavior and DFT calculations indicate the following mechanism of CO_2 binding for $Mebipy^+$ and the related $Prbipy^+$ (Scheme 6). First, the $Mebipy^+$ is reduced by one electron to form a neutral Mebipy*. In the presence of CO_2, $Mebipy^\bullet$ species undergoes disproportionation to form $Mebipy^+$ and $Mebipy^-$. The latter reacts with CO_2 to form $Mebipy–CO_2^-$, which results in a disappearance of the more cathodic redox event. The CO_2 adduct can then be electrochemically oxidized by two electrons to return the parent $Mebipy^+$ cation. For these monoalkylated bipyridinium species, the stoichiometry thus requires two electrons due to the disproportionation event that occurs to capture one molecule of CO_2.

Scheme 6. Reduction of $MeBipy^+$, disproportionation of $Mebipy^\bullet$, and CO_2 binding to $Mebipy^-$

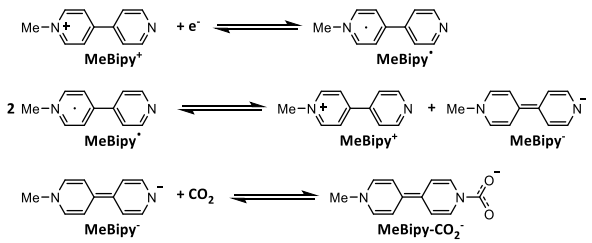

Buttry and coworkers also studied the related non-alkylated compound, 4-,4'-bipyridine (bipy).[160] The one electron reduction of bipy produces the radical anion, $bipy^{\bullet-}$, which quickly binds to CO_2. Following oxidation of the $bipy–CO_2^{\bullet-}$ adduct, CO_2 is released and bipy is regenerated. This mechanism differs from the monoalkylated bipyridinium compounds. One equivalent of electrons is sufficient for capturing a single equivalent of CO_2 due to the more nucleophilic radical anion, which readily binds to CO_2 after a single reduction. In the ionic liquid BMF TFSI under a N_2 atmosphere, reduction of bipy to $bipy^{\bullet-}$ is a one

electron reversible couple at -2.25 V vs ferrocene. In a solution saturated with CO_2, the reduction peak for bipy$^{\bullet-}$ shifts from -2.3 V to -2.05 V vs ferrocene displaying strong binding between bipy$^{\bullet-}$ CO_2. The bipy–$CO_2^{\bullet-}$ is oxidized at -1.35 V vs ferrocene, a substantial positive shift due to the very stable N–C bond formed in the adduct. The large potential difference between reduction and oxidation of this adduct is a crucial component as it can impact the total energy for the bipy–CO_2 capture release cycle.

Computations were also carried out to elucidate the reaction mechanism of CO_2 capture by 4,4'-bipyridine.[160] Utilizing DFT (B3LYP and M062X) with the implicit continuum solvation model, the computations revealed that a stable adduct is formed between the 4,4'-bipyridine anion radical and the CO_2 molecule, with the ΔG_0 = –43.9 kJ/mol.[160] The release of the CO_2 molecule was then accomplished by re-oxidation of the adduct, presumably yielding a zwitterionic intermediate, which is susceptible to a facile decarboxylation.

5.2.4 Dithiols.

Buttry and coworkers also described the use of thiolates as redox carriers.[136] Prior to this study, there were few reports of S-bound terminal thiocarbonates, and no description of the electrochemical behavior of thiocarbonate.[161, 162] Buttry and coworkers specifically looked at benzyldisulfide (BDS) for direct eCCC where they observed that from one equivalent of BDS, a two-electron reduction results in two equivalents of nucleophilic benzylthiolate that can react with one CO_2 molecule forming a *S*-benzylthiocarbonate (Scheme 7). Using DFT (B3LYP), CO_2 capture is estimated to have a binding energy of -66 kJ mol^{-1}. Computations were also used to elucidate the CO_2 release step. The authors proposed that CO_2 release should follow the oxidation of thiocarbonate due to a significant electron density localized at the S–C bond of thiol and CO_2 in the redox-active molecular orbital (RAMO). Removing the electron from RAMO upon oxidation should thus lead to the bond destabilization and the rapid CO_2 release. From the overall mechanism, a stoichiometry of one CO_2 captured per one electron transferred to BDS was found, which theoretically allows for capture of two CO_2 molecules per each BDS.

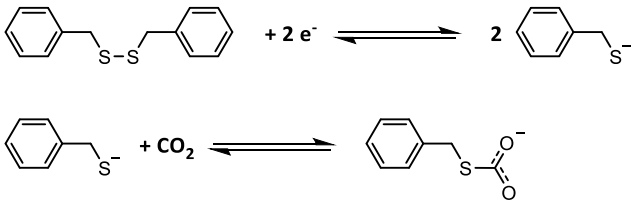

Scheme 7. Mechanism of CO_2 capture via reduction of benzyldisulfide.

Harris and Bushnell added to the BDS study from Buttry and coworkers using DFT to assess solvent effects while also exploring the use of other benzyldichalcogenide compounds.[163] Pursuant to the dielectric constant of different solvents, the absolute reduction potential and the interaction energy for benzylthiolate-CO_2 binding were exhibited to range between 2.7 to 3.4 V and –30 to –40 kJ/mol,

respectively. They also found that chalcogenide atom significantly impacted the oxidation/CO_2 release step. The CO_2 adducts formed in systems involving benzyldiselenide and benzylditelluride had less positive absolute reduction potentials compared to benzyldisulfide (BDS). Thus, the authors suggested using benzyl telluride and benzyl selenide as the potential eCCC agents, as they should have a better peak-to-peak separation between the CO_2 capture and CO_2 release potentials. However, other factors, such as toxicity and availability, must also be considered.

5.3 Cell and System Design.

To date, most studies employing redox-active capture molecules for direct eCCC have consisted of proof-of-concept, cyclic voltammetry and/or bulk electrolysis experiments focused on characterizing capture species-electrolyte pairs in well-defined and controlled environments. Only a few studies have incorporated these molecules into an engineered cell design with flowing gas streams. In the electro-swing absorption (ESA) system previously introduced, the redox-active capture agent is immobilized on the electrode surface and activated via polarization to capture CO_2.[147,148] A counter electrode, which is the positive electrode during the absorption phase, is used to complete the flow of electrons (**Figure 7**). Once the negative electrode is saturated with CO_2 the polarity of the cell is deliberately reversed, deactivating the capture agent at the now positive electrode in order to release CO_2 by desorption. Systems with the capture agent immobilized on the solid electrode require the feed gas stream, containing CO_2, to be fed directly to the electrode. Between both electrodes is a membrane/separator imbibed with the liquid electrolyte, which allows the porous electrode to become wetted with a liquid film. This architecture facilitates the flow of ionic current throughout the 3D electrode structure to the electrochemical reaction sites. In a flowing gas operation scheme, the feed gas containing CO_2 is fed through a parallel flow-field, and thus CO_2 must diffuse laterally through both the porous media and the liquid film to react with the activated quinone species.[147, 148] In these ESA systems, which employ electrodes that require three-phase contact, utilization of the carrier species is likely to be controlled by the CO_2 mass transfer rate through the porous electrode and liquid film, which may be orders of magnitude lower than both the electrochemical and chemical (absorption and desorption) reaction rates. Accordingly, demonstrations for ESA systems have been limited to low current density operation (≤ 2 mA cm^{-2}).[148] Additionally, it has been shown both experimentally and computationally that quinone utilization in a given cycle length is strongly dependent on the CO_2 concentration in the feed gas, which affects the driving force for film diffusion.[147]

More recently, use of a liquid quinone for direct eCCC was demonstrated in a redox flow battery type system, similar to what was described for some of the pH-swing setups in Section 3.3 (and depicted in

Figure 4). By employing two electrochemical cells, continuous, rather than cyclic, CO_2 capture was performed in one system. More specifically, one cell was used for sorbent activation and the other for deactivation with the absorption/desorption steps carried out in external units.

5.4 Experimental Methods for Measuring CO_2 Binding Affinities.

Determination of $K_{1(\mathrm{R}^{n-})}$ and $K_{2(\mathrm{R})}$ values for the active and resting states of redox carriers can be determined utilizing numerous methods. Unique to redox carriers however, electrochemical methods can be employed dependent on the mechanism. For a system that employs an EC mechanism (electron transfer followed by chemical step), or EEC mechanism, carrier CO_2 binding constants ($K_{1(\mathrm{R}^{n-})}$ values between 100 and 10^{15}) can be measured using the observed shift in the half-wave potential, $E_{1/2}$, recorded in the presence and absence of a known concentration of CO_2 by applying eq. 11.[131, 164]

$$E_{1/2} = E^{o\prime} + \frac{R_\mathrm{u}T}{nF}\ln\left(K_{1(\mathrm{R}^{n-})}\right) + q\frac{RT}{nF}\ln\left[\mathrm{CO_2}\right] \qquad \textbf{Eq. 11}$$

Where R_u is the universal gas constant, T is temperature, F is Faraday's constant, and n is the number of electrons being passed in the redox event. The number of CO_2 molecules that are bound during the chemical step is represented by the term q (typically, q = 1 for most carriers, but can be determined via other spectroscopic or voltammetric techniques[124, 137, 165]). $E^{o\prime}$ is the half-wave potential in the absence of CO_2, while $E_{1/2}$ represents the half-wave potential in the presence of a known CO_2 concentration in solution ($[\mathrm{CO_2}]$). This approach can be highly beneficial as it does not require isolation of the active state carrier, which can often be unstable or difficult to isolate cleanly. For an EC mechanism where $K_{1(\mathrm{R}^{n-})}$ values are larger than 10^{15}, the change in potential can be measured using the open circuit potential, with a varied range of CO_2 concentrations. In this case, the active state carrier must be formed chemically or electrochemically. The $E_{1/2}$ value from eq. 11 would refer to the open circuit potential under a known concentration of CO_2. The $E^{o\prime}$ value would refer to the open circuit potential in the absence of CO_2. The y-intercept of the linear relationship of the change in open circuit potential versus the natural log of the concentration of CO_2 in solution can be used to find the binding constant.

Values of K_{CO2} for redox-carriers can be also be determined using more common spectroscopic or physical techniques, depending on the magnitude of $K_{1(\mathrm{R}^{n-})}$ and solubility of the carrier. These techniques include, but are not limited to: NMR and electronic absorption spectroscopy, gravimetry, and gas uptake experiments.[124, 137, 166, 167]

For a system that does not utilize an EC or EEC mechanism, the binding constant can be estimated using the electronic absorption spectra at various CO_2 concentrations.[124] The carrier must be in the active state in order to use this method. In previous work, the electronic absorption spectra were studied as a

function of CO_2 concentration, and analyzed by the Benesi-Hildebrand method to find the equilibrium constant.[168]

6. Concluding Remarks and Outlook.

The use of electrochemical CO_2 capture and concentration was initially reported in literature in the 1960's. In the intervening time frame, several different concepts and architectures have been proposed, with significant advancements occurring over the last decade. Some of these systems already operate with estimated energetic efficiencies rivaling state-of-the-art systems in the laboratory setting. These results have demonstrated the promise of eCCC, but also outline scientific challenges that, if addressed, would accelerate implementation and widespread use. Long term stability still represents a challenge in most eCCC systems. Most pH swing, EMAR, and redox carrier systems are specifically sensitive to oxygen, which is commonly present in dilute CO_2 streams. Modifying these systems to work at milder electrochemical potentials would likely be beneficial for oxygen stability, as well as engineering design approaches (e.g., implementation of oxygen separation). Stability of current chemistries towards water vapor (for non-aqueous systems) and other components in a CO_2-containing streams is also not clear.

Most studies have focused on improving the chemistry of eCCC systems, such as the carrier species and electrolyte, for proof-of-concept experiments. However, design and operation of the electrochemical cell will also greatly impact performance of the system, including optimizing for high separation capacity and balancing overall energetics versus Faradaic efficiencies. Other considerations that will be required for overall operation include selection of cell components (electrodes, membrane/separator, flow channels) and operating conditions, and the costs associated with these. The ideal properties and materials are not well understood and will likely depend on the specific application.

Interest in more efficient and scalable eCCC has been motivated by the urgency to decarbonize current industries to operate with minimal or no carbon emissions, and direct air capture to achieve carbon negative technologies. With continued research investment to synergistically address the chemistry and engineering challenges, eCCC can more quickly become a reality.

Acknowledgements

We would like to thank the Sloan Foundation for funding the authors of this review.

Conflicts of Interest

There are no conflicts of interest to declare.

Citations

(1) IPCC. *Climate Change 2022: Mitigation of Climate Change. Contribution of Working Group III to the Sixth Assessment Report of the Intergovernmental Panel on Climate Change*; 10.1017/9781009157926; Cambridge, UK and New York, NY, 2022.
(2) IEA. *Global Energy Review: CO2 Emissions in 2021*; Paris, 2022. https://www.iea.org/reports/global-energy-review-co2-emissions-in-2021-2.
(3) Friedlingstein, P.; Jones, M. W.; O'Sullivan, M.; Andrew, R. M.; Bakker, D. C. E.; Hauck, J.; Le Quéré, C.; Peters, G. P.; Peters, W.; Pongratz, J.; et al. Global Carbon Budget 2021. *Earth Syst. Sci. Data* **2022**, *14* (4), 1917-2005. DOI: 10.5194/essd-14-1917-2022.
(4) Huebscher, R. G. B., A. D. Electrochemical Concentration and Separation of Carbon Dioxide for Advanced Life Supprot Systems - Carbonation Cell System. *SAE Technical Papers* **1969**, 2164 - 2170.
(5) Rogelj, J.; den Elzen, M.; Höhne, N.; Fransen, T.; Fekete, H.; Winkler, H.; Schaeffer, R.; Sha, F.; Riahi, K.; Meinshausen, M. Paris Agreement climate proposals need a boost to keep warming well below 2 °C. *Nature* **2016**, *534* (7609), 631-639. DOI: 10.1038/nature18307.
(6) CO2 and Greenhouse Gas Emissions. https://ourworldindata.org/co2-and-other-greenhouse-gas-emissions (accessed September 2022).
(7) Metz, B.; Davidson, O.; de Coninck, H.; Loos, M.; Meyer, L. IPCC Special Report on Carbon dioxide Capture and Storage. *Policy Stud.* **2005**.
(8) https://ourworldindata.org/emissions-by-sector#co2-emissions-by-sector (accessed.
(9) IEA. *Net Zero by 2050*; Paris, 2021. https://www.iea.org/reports/net-zero-by-2050.
(10) Rogelj, J.; Popp, A.; Calvin, K. V.; Luderer, G.; Emmerling, J.; Gernaat, D.; Fujimori, S.; Strefler, J.; Hasegawa, T.; Marangoni, G.; et al. Scenarios towards limiting global mean temperature increase below 1.5 °C. *Nature Climate Change* **2018**, *8* (4), 325-332. DOI: 10.1038/s41558-018-0091-3.
(11) Institute, G. C. *Global Status of CCS 2021*; 2021. https://www.globalccsinstitute.com/resources/global-status-report/.
(12) Institute, G. C. https://co2re.co/FacilityData (accessed.
(13) Tavoni, M.; van der Zwaan, B. Nuclear Versus Coal plus CCS: a Comparison of Two Competitive Base-Load Climate Control Options. *Environmental Modeling & Assessment* **2011**, *16* (5), 431-440. DOI: 10.1007/s10666-011-9259-1.
(14) Chu, S.; Majumdar, A. Opportunities and challenges for a sustainable energy future. *Nature* **2012**, *488* (7411), 294-303, 10.1038/nature11475.
(15) Lackner, K. S.; Brennan, S.; Matter, J. M.; Park, A.-H. A.; Wright, A.; van der Zwaan, B. The urgency of the development of CO₂ capture from ambient air. *Proceedings of the National Academy of Sciences* **2012**, *109* (33), 13156-13162. DOI: 10.1073/pnas.1108765109.
(16) IEA. *Direct Air Capture*; Paris, 2021. https://www.iea.org/reports/direct-air-capture.
(17) Hammond, G. P.; Akwe, S. S. O.; Williams, S. Techno-economic appraisal of fossil-fuelled power generation systems with carbon dioxide capture and storage. *Energy* **2011**, *36* (2), 975-984. DOI: https://doi.org/10.1016/j.energy.2010.12.012.
(18) House, K. Z.; Baclig, A. C.; Ranjan, M.; van Nierop, E. A.; Wilcox, J.; Herzog, H. J. Economic and energetic analysis of capturing CO₂ from ambient air. *Proceedings of the National Academy of Sciences* **2011**, *108* (51), 20428-20433. DOI: doi:10.1073/pnas.1012253108.
(19) Chao, C.; Deng, Y.; Dewil, R.; Baeyens, J.; Fan, X. Post-combustion carbon capture. *Renewable and Sustainable Energy Reviews* **2021**, *138*, 110490. DOI: https://doi.org/10.1016/j.rser.2020.110490.
(20) Raza, A.; Gholami, R.; Rezaee, R.; Rasouli, V.; Rabiei, M. Significant aspects of carbon capture and storage – A review. *Petroleum* **2019**, *5* (4), 335-340. DOI: https://doi.org/10.1016/j.petlm.2018.12.007.
(21) Wang, X.; Song, C. Carbon Capture From Flue Gas and the Atmosphere: A Perspective. *Frontiers in Energy Research* **2020**, *8*, Review. DOI: 10.3389/fenrg.2020.560849.

(22) Yu, C.-H.; Huang, C.-H.; Tan, C.-S. A Review of CO2 Capture by Absorption and Adsorption. *Aerosol and Air Quality Research* **2012**, *12* (5), 745-769. DOI: 10.4209/aaqr.2012.05.0132.
(23) House, K. Z.; Harvey, C. F.; Aziz, M. J.; Schrag, D. P. The energy penalty of post-combustion CO2 capture & storage and its implications for retrofitting the U.S. installed base. *Energy & Environmental Science* **2009**, *2* (2), 193-205. DOI: 10.1039/B811608C.
(24) Abu-Zahra, M. R. M.; Schneiders, L. H. J.; Niederer, J. P. M.; Feron, P. H. M.; Versteeg, G. F. CO2 capture from power plants: Part I. A parametric study of the technical performance based on monoethanolamine. *International Journal of Greenhouse Gas Control* **2007**, *1* (1), 37-46. DOI: https://doi.org/10.1016/S1750-5836(06)00007-7.
(25) Goto, K.; Kodama, S.; Okabe, H.; Fujioka, Y. Energy Performance of New Amine-Based Solvents for CO₂ Capture from Blast Furnace Gas. In *Recent Advances in Post-Combustion CO₂ Capture Chemistry*, ACS Symposium Series, Vol. 1097; American Chemical Society, 2012; pp 317-331.
(26) Singh, A.; Stéphenne, K. Shell Cansolv CO2 capture technology: Achievement from First Commercial Plant. *Energy Procedia* **2014**, *63*, 1678-1685. DOI: https://doi.org/10.1016/j.egypro.2014.11.177.
(27) Yulia, F.; Sofianita, R.; Prayogo, K.; Nasruddin, N. Optimization of post combustion CO2 absorption system monoethanolamine (MEA) based for 320 MW coal-fired power plant application – Exergy and exergoenvironmental analysis. *Case Studies in Thermal Engineering* **2021**, *26*, 101093. DOI: https://doi.org/10.1016/j.csite.2021.101093.
(28) Rochelle, G.; Chen, E.; Freeman, S.; Van Wagener, D.; Xu, Q.; Voice, A. Aqueous piperazine as the new standard for CO2 capture technology. *Chemical Engineering Journal* **2011**, *171* (3), 725-733. DOI: https://doi.org/10.1016/j.cej.2011.02.011.
(29) Boot-Handford, M. E.; Abanades, J. C.; Anthony, E. J.; Blunt, M. J.; Brandani, S.; Mac Dowell, N.; Fernández, J. R.; Ferrari, M.-C.; Gross, R.; Hallett, J. P.; et al. Carbon capture and storage update. *Energy & Environmental Science* **2014**, *7* (1), 130-189, 10.1039/C3EE42350F. DOI: 10.1039/C3EE42350F.
(30) Rochelle, G. T. Amine Scrubbing for CO₂ Capture. *Science* **2009**, *325* (5948), 1652-1654. DOI: 10.1126/science.1176731.
(31) Wilcox, J. *Carbon Capture*; Springer, 2012.
(32) Institute, G. C. *State of the Art: CCS Technologies 2022*; 2022. https://www.globalccsinstitute.com/wp-content/uploads/2022/05/State-of-the-Art-CCS-Technologies-2022.pdf.
(33) Baylin-Stern, A. B., N. *Is carbon capture too expensive?*; Paris, 2021. https://www.iea.org/commentaries/is-carbon-capture-too-expensive.
(34) Fasihi, M.; Efimova, O.; Breyer, C. Techno-economic assessment of CO2 direct air capture plants. *Journal of Cleaner Production* **2019**, *224*, 957-980. DOI: https://doi.org/10.1016/j.jclepro.2019.03.086.
(35) McQueen, N.; Psarras, P.; Pilorgé, H.; Liguori, S.; He, J.; Yuan, M.; Woodall, C. M.; Kian, K.; Pierpoint, L.; Jurewicz, J.; et al. Cost Analysis of Direct Air Capture and Sequestration Coupled to Low-Carbon Thermal Energy in the United States. *Environmental Science & Technology* **2020**, *54* (12), 7542-7551. DOI: 10.1021/acs.est.0c00476.
(36) Lackner, K. S.; Azarabadi, H. Buying down the Cost of Direct Air Capture. *Ind. Eng. Chem. Res.* **2021**, *60* (22), 8196-8208. DOI: 10.1021/acs.iecr.0c04839.
(37) *Global Status of CCS: 2019*; Global CCS Institute, Australia, 2019.
(38) Lackner, K. S. The thermodynamics of direct air capture of carbon dioxide. *Energy* **2013**, *50*, 38-46. DOI: https://doi.org/10.1016/j.energy.2012.09.012.
(39) Stern, M. C.; Simeon, F.; Herzog, H.; Hatton, T. A. Post-combustion carbon dioxide capture using electrochemically mediated amine regeneration. *Energy & Environ. Sci.* **2013**, *6* (8), 2505-2517, 10.1039/C3EE41165F. DOI: 10.1039/C3EE41165F.

(40) Stern, M. C.; Simeon, F.; Hammer, T.; Landes, H.; Herzog, H. J.; Alan Hatton, T. Electrochemically mediated separation for carbon capture. *Energy Procedia* **2011**, *4*, 860-867. DOI: https://doi.org/10.1016/j.egypro.2011.01.130.
(41) Shaw, R. A.; Hatton, T. A. Electrochemical CO2 capture thermodynamics. *International Journal of Greenhouse Gas Control* **2020**, *95*, 102878. DOI: https://doi.org/10.1016/j.ijggc.2019.102878.
(42) Rheinhardt, J. H.; Singh, P.; Tarakeshwar, P.; Buttry, D. A. Electrochemical capture and release of carbon dioxide. *ACS Energy Letters* **2017**, *2* (2), 454-461. DOI: 10.1021/acsenergylett.6b00608.
(43) Barlow, J. M.; Clarke, L. E.; Zhang, Z.; Bím, D.; Ripley, K. M.; Zito, A.; Brushett, F. R.; Alexandrova, A. N.; Yang, J. Y. Molecular design of redox carriers for electrochemical CO2 capture and concentration. *Chem. Soc. Rev.* **2022**, 10.1039/D2CS00367H. DOI: 10.1039/D2CS00367H.
(44) Dell'Osso, L.; Ruder, J. M.; Winnick, J. Mixed-Gas Adsorption and Vacuum Desorption of Carbon Dioxide on Molecular Sieve. Bed Performance and Data Analysis. *Industrial & Engineering Chemistry Process Design and Development* **1969**, *8* (4), 477-482. DOI: 10.1021/i260032a007.
(45) Martin, R. B. Carbon dioxide control for manned spacecraft. *Aerospace medicine* **1968**, *39 9*, 937-941.
(46) Wynveen, R. A. Q., P. D. Electrochemical carbon dioxide concentrating system. In *ASME Life Support Conference*, San Francisco, CA, 1971.
(47) Wynveen, R. A. S., F. H.; Powell, J. D. *One-man self-contained CO concentrator system*; NASA CR-114426; 1972.
(48) Winnick, J.; Marshall, R. D.; Schubert, F. H. An Electrochemical Device for Carbon Dioxide Concentration. I. System Design and Performance. *Industrial & Engineering Chemistry Process Design and Development* **1974**, *13* (1), 59-63. DOI: 10.1021/i260049a011.
(49) Eisaman, M. D. S., D. E.; Amic, S.; Larner, D.; Zesch, J.; Torrest, F.; Littau, K. Energy-efficient electrochemical CO2 capture from the atmosphere. *Clean Technology* **2009**, 175-178.
(50) Winnick, J.; Toghiani, H.; Quattrone, P. D. Carbon dioxide concentration for manned spacecraft using a molten carbonate electrochemical cell. *AIChE J.* **1982**, *28* (1), 103-111. DOI: https://doi.org/10.1002/aic.690280115.
(51) Weaver, J. L.; Winnick, J. The Molten Carbonate Carbon Dioxide Concentrator: Cathode Performance at High CO 2 Utilization. *J. Electrochem. Soc.* **1983**, *130* (1), 20-28. DOI: 10.1149/1.2119661.
(52) Kang, M. P.; Winnick, J. Concentration of carbon dioxide by a high-temperature electrochemical membrane cell. *J. Appl. Electrochem.* **1985**, *15* (3), 431-439. DOI: 10.1007/BF00615996.
(53) Sharifian, R.; Wagterveld, R. M.; Digdaya, I. A.; Xiang, C.; Vermaas, D. A. Electrochemical carbon dioxide capture to close the carbon cycle. *Energy & Environmental Science* **2021**, *14* (2), 781-814, 10.1039/D0EE03382K. DOI: 10.1039/D0EE03382K.
(54) Ye, W.; Huang, J.; Lin, J.; Zhang, X.; Shen, J.; Luis, P.; Van der Bruggen, B. Environmental evaluation of bipolar membrane electrodialysis for NaOH production from wastewater: Conditioning NaOH as a CO2 absorbent. *Sep. Purif. Technol.* **2015**, *144*, 206-214. DOI: https://doi.org/10.1016/j.seppur.2015.02.031.
(55) Eisaman, M. D.; Alvarado, L.; Larner, D.; Wang, P.; Garg, B.; Littau, K. A. CO2 separation using bipolar membrane electrodialysis. *Energy & Environmental Science* **2011**, *4* (4), 1319-1328, 10.1039/C0EE00303D. DOI: 10.1039/C0EE00303D.
(56) Eisaman, M. D.; Alvarado, L.; Larner, D.; Wang, P.; Littau, K. A. CO2 desorption using high-pressure bipolar membrane electrodialysis. *Energy & Environmental Science* **2011**, *4* (10), 4031-4037, 10.1039/C1EE01336J. DOI: 10.1039/C1EE01336J.
(57) Sabatino, F.; Mehta, M.; Grimm, A.; Gazzani, M.; Gallucci, F.; Kramer, G. J.; van Sint Annaland, M. Evaluation of a Direct Air Capture Process Combining Wet Scrubbing and Bipolar Membrane Electrodialysis. *Ind. Eng. Chem. Res.* **2020**, *59* (15), 7007-7020. DOI: 10.1021/acs.iecr.9b05641.

(58) Eisaman, M. D.; Parajuly, K.; Tuganov, A.; Eldershaw, C.; Chang, N.; Littau, K. A. CO2 extraction from seawater using bipolar membrane electrodialysis. *Energy & Environmental Science* **2012**, *5* (6), 7346-7352, 10.1039/C2EE03393C. DOI: 10.1039/C2EE03393C.
(59) Datta, S.; Henry, M. P.; Lin, Y. J.; Fracaro, A. T.; Millard, C. S.; Snyder, S. W.; Stiles, R. L.; Shah, J.; Yuan, J.; Wesoloski, L.; et al. Electrochemical CO2 Capture Using Resin-Wafer Electrodeionization. *Ind. Eng. Chem. Res.* **2013**, *52* (43), 15177-15186. DOI: 10.1021/ie402538d.
(60) Warren, J. J.; Tronic, T. A.; Mayer, J. M. Thermochemistry of Proton-Coupled Electron Transfer Reagents and its Implications. *Chemical Reviews* **2010**, *110* (12), 6961-7001. DOI: 10.1021/cr100085k.
(61) Winsberg, J.; Hagemann, T.; Janoschka, T.; Hager, M. D.; Schubert, U. S. Redox-Flow Batteries: From Metals to Organic Redox-Active Materials. *Angewandte Chemie International Edition* **2017**, *56* (3), 686-711. DOI: 10.1002/anie.201604925.
(62) Huang, C.; Liu, C.; Wu, K.; Yue, H.; Tang, S.; Lu, H.; Liang, B. CO2 Capture from Flue Gas Using an Electrochemically Reversible Hydroquinone/Quinone Solution. *Energy Fuels* **2019**, *33* (4), 3380-3389. DOI: 10.1021/acs.energyfuels.8b04419.
(63) Huynh, M. T.; Anson, C. W.; Cavell, A. C.; Stahl, S. S.; Hammes-Schiffer, S. Quinone 1 e– and 2 e–/2 H+ Reduction Potentials: Identification and Analysis of Deviations from Systematic Scaling Relationships. *J. Am. Chem. Soc.* **2016**, *138* (49), 15903-15910. DOI: 10.1021/jacs.6b05797.
(64) Yang, B.; Hoober-Burkhardt, L.; Krishnamoorthy, S.; Murali, A.; Prakash, G. K. S.; Narayanan, S. R. High-Performance Aqueous Organic Flow Battery with Quinone-Based Redox Couples at Both Electrodes. *J. Electrochem. Soc.* **2016**, *163* (7), A1442-A1449. DOI: 10.1149/2.1371607jes.
(65) Lin, K.; Gómez-Bombarelli, R.; Beh, E. S.; Tong, L.; Chen, Q.; Valle, A.; Aspuru-Guzik, A.; Aziz, M. J.; Gordon, R. G. A redox-flow battery with an alloxazine-based organic electrolyte. *Nature Energy* **2016**, *1* (9), 16102. DOI: 10.1038/nenergy.2016.102.
(66) Lin, K.; Chen, Q.; Gerhardt, M. R.; Tong, L.; Kim, S. B.; Eisenach, L.; Valle, A. W.; Hardee, D.; Gordon, R. G.; Aziz, M. J.; et al. Alkaline quinone flow battery. *Science* **2015**, *349* (6255), 1529-1532. DOI: 10.1126/science.aab3033.
(67) Er, S.; Suh, C.; Marshak, M. P.; Aspuru-Guzik, A. Computational design of molecules for an all-quinone redox flow battery. *Chemical Science* **2015**, *6* (2), 885-893, 10.1039/C4SC03030C. DOI: 10.1039/C4SC03030C.
(68) Watkins, J. D.; Siefert, N. S.; Zhou, X.; Myers, C. R.; Kitchin, J. R.; Hopkinson, D. P.; Nulwala, H. B. Redox-Mediated Separation of Carbon Dioxide from Flue Gas. *Energy Fuels* **2015**, *29* (11), 7508-7515. DOI: 10.1021/acs.energyfuels.5b01807.
(69) Jin, S.; Wu, M.; Gordon, R. G.; Aziz, M. J.; Kwabi, D. G. pH swing cycle for CO2 capture electrochemically driven through proton-coupled electron transfer. *Energy & Environmental Science* **2020**, *13* (10), 3706-3722, 10.1039/D0EE01834A. DOI: 10.1039/D0EE01834A.
(70) Xie, H.; Wu, Y.; Liu, T.; Wang, F.; Chen, B.; Liang, B. Low-energy-consumption electrochemical CO2 capture driven by biomimetic phenazine derivatives redox medium. *Applied Energy* **2020**, *259*, 114119. DOI: https://doi.org/10.1016/j.apenergy.2019.114119.
(71) Seo, H.; Rahimi, M.; Hatton, T. A. Electrochemical Carbon Dioxide Capture and Release with a Redox-Active Amine. *J. Am. Chem. Soc.* **2022**, *144* (5), 2164-2170. DOI: 10.1021/jacs.1c10656.
(72) Yamaguchi, A.; Inuzuka, R.; Takashima, T.; Hayashi, T.; Hashimoto, K.; Nakamura, R. Regulating proton-coupled electron transfer for efficient water splitting by manganese oxides at neutral pH. *Nature Communications* **2014**, *5* (1), 4256. DOI: 10.1038/ncomms5256.
(73) Xie, H.; Jiang, W.; Liu, T.; Wu, Y.; Wang, Y.; Chen, B.; Niu, D.; Liang, B. Low-Energy Electrochemical Carbon Dioxide Capture Based on a Biological Redox Proton Carrier. *Cell Reports Physical Science* **2020**, *1* (5), 100046. DOI: https://doi.org/10.1016/j.xcrp.2020.100046.
(74) Costentin, C. Electrochemical Approach to the Mechanistic Study of Proton-Coupled Electron Transfer. *Chemical Reviews* **2008**, *108* (7), 2145-2179. DOI: 10.1021/cr068065t.

(75) Song, N.; Gagliardi, C. J.; Binstead, R. A.; Zhang, M.-T.; Thorp, H.; Meyer, T. J. Role of Proton-Coupled Electron Transfer in the Redox Interconversion between Benzoquinone and Hydroquinone. *J. Am. Chem. Soc.* **2012**, *134* (45), 18538-18541. DOI: 10.1021/ja308700t.
(76) Michael, A.; David G., K. *pH Swing Cycle for CO2 Capture Electrochemically Driven through Proton-Coupled Electron Transfer*; 2019. DOI: 10.26434/chemrxiv.7853414.v1.
(77) Hollas, A.; Wei, X.; Murugesan, V.; Nie, Z.; Li, B.; Reed, D.; Liu, J.; Sprenkle, V.; Wang, W. A biomimetic high-capacity phenazine-based anolyte for aqueous organic redox flow batteries. *Nature Energy* **2018**, *3* (6), 508-514. DOI: 10.1038/s41560-018-0167-3.
(78) Leitz, F. B.; Marinčić, L. Enhanced mass transfer in electrochemical cells using turbulence promoters. *J. Appl. Electrochem.* **1977**, *7* (6), 473-484. DOI: 10.1007/BF00616758.
(79) Rahimi, M.; Catalini, G.; Hariharan, S.; Wang, M.; Puccini, M.; Hatton, T. A. Carbon Dioxide Capture Using an Electrochemically Driven Proton Concentration Process. *Cell Reports Physical Science* **2020**, *1* (4), 100033. DOI: https://doi.org/10.1016/j.xcrp.2020.100033.
(80) Rahimi, M.; Catalini, G.; Puccini, M.; Hatton, T. A. Bench-scale demonstration of CO2 capture with an electrochemically driven proton concentration process. *RSC Advances* **2020**, *10* (29), 16832-16843. DOI: 10.1039/D0RA02450C.
(81) Mondal, M. K.; Balsora, H. K.; Varshney, P. Progress and trends in CO2 capture/separation technologies: A review. *Energy* **2012**, *46* (1), 431-441. DOI: https://doi.org/10.1016/j.energy.2012.08.006.
(82) Wang, M.; Herzog, H. J.; Hatton, T. A. CO2 Capture Using Electrochemically Mediated Amine Regeneration. *Ind. Eng. Chem. Res.* **2020**, *59* (15), 7087-7096. DOI: 10.1021/acs.iecr.9b05307.
(83) Stern, M. C. Electrochemically-mediated amine regeneration for carbon dioxide separations. Masschusetts Institute of Technology, 2013.
(84) Wang, M.; Hariharan, S.; Shaw, R. A.; Hatton, T. A. Energetics of electrochemically mediated amine regeneration process for flue gas CO2 capture. *International Journal of Greenhouse Gas Control* **2019**, *82*, 48-58. DOI: https://doi.org/10.1016/j.ijggc.2018.12.028.
(85) Stern, M. C.; Simeon, F.; Herzog, H.; Hatton, T. A. Post-combustion carbon dioxide capture using electrochemically mediated amine regeneration. *Energy & Environmental Science* **2013**, *6* (8), 2505-2517. DOI: 10.1039/C3EE41165F.
(86) Stern, M. C.; Hatton, T. A. Bench-scale demonstration of CO2 capture with electrochemically-mediated amine regeneration. *RSC Advances* **2014**, *4* (12), 5906-5914. DOI: 10.1039/C3RA46774K.
(87) Wang, M.; Rahimi, M.; Kumar, A.; Hariharan, S.; Choi, W.; Hatton, T. A. Flue gas CO2 capture via electrochemically mediated amine regeneration: System design and performance. *Applied Energy* **2019**, *255*, 113879. DOI: https://doi.org/10.1016/j.apenergy.2019.113879.
(88) Eltayeb, A. O.; Stern, M. C.; Herzog, H.; Hatton, T. A. Energetics of Electrochemically-mediated Amine Regeneration. *Energy Procedia* **2014**, *63*, 595-604. DOI: https://doi.org/10.1016/j.egypro.2014.11.064.
(89) Liu, G. X.; Yu, Y. S.; Hong, Y. T.; Zhang, Z. X.; Wei, J. J.; Wang, G. G. X. Identifying electrochemical effects in a thermal–electrochemical co-driven system for CO2 capture. *Phys. Chem. Chem. Phys.* **2017**, *19* (20), 13230-13244. DOI: 10.1039/C7CP01035D.
(90) Eltayeb, A. E. Analysis and Design of Electrochemically-Mediated Carbon Dioxide Separation. Massachusetts Institute of Technology, Cambridge, MA, 2017.
(91) Wang, M.; Hatton, T. A. Flue Gas CO2 Capture via Electrochemically Mediated Amine Regeneration: Desorption Unit Design and Analysis. *Ind. Eng. Chem. Res.* **2020**, *59* (21), 10120-10129. DOI: 10.1021/acs.iecr.0c00790.
(92) Colli, A. N.; Toelzer, R.; Bergmann, M. E. H.; Bisang, J. M. Mass-transfer studies in an electrochemical reactor with a small interelectrode gap. *Electrochim. Acta* **2013**, *100*, 78-84. DOI: https://doi.org/10.1016/j.electacta.2013.03.134.

(93) Castañeda, L. F.; Walsh, F. C.; Nava, J. L.; Ponce de León, C. Graphite felt as a versatile electrode material: Properties, reaction environment, performance and applications. *Electrochim. Acta* **2017**, *258*, 1115-1139. DOI: https://doi.org/10.1016/j.electacta.2017.11.165.
(94) Babic, U.; Suermann, M.; Büchi, F. N.; Gubler, L.; Schmidt, T. J. Critical Review—Identifying Critical Gaps for Polymer Electrolyte Water Electrolysis Development. *J. Electrochem. Soc.* **2017**, *164* (4), F387-F399. DOI: 10.1149/2.1441704jes.
(95) Moussallem, I.; Jörissen, J.; Kunz, U.; Pinnow, S.; Turek, T. Chlor-alkali electrolysis with oxygen depolarized cathodes: history, present status and future prospects. *J. Appl. Electrochem.* **2008**, *38* (9), 1177-1194. DOI: 10.1007/s10800-008-9556-9.
(96) Pollard, R.; Newman, J. Transient behaviour of porous electrodes with high exchange current densities. *Electrochim. Acta* **1980**, *25* (3), 315-321. DOI: https://doi.org/10.1016/0013-4686(80)90012-2.
(97) Shaw, R. A. Modeling and Design for Electrochemical Carbon Dioxide Capture Systems. Massachusetts Institute of Technology, Cambridge, MA, 2019.
(98) Pletcher, D.; Walsh, F. C. *Industrial Electrochemistry*; Springer Netherlands, 1990.
(99) Yang, H. S.; Park, J. H.; Ra, H. W.; Jin, C.-S.; Yang, J. H. Critical rate of electrolyte circulation for preventing zinc dendrite formation in a zinc–bromine redox flow battery. *J. Power Sources* **2016**, *325*, 446-452. DOI: https://doi.org/10.1016/j.jpowsour.2016.06.038.
(100) Stowe, H. M.; Hwang, G. S. Fundamental Understanding of CO2 Capture and Regeneration in Aqueous Amines from First-Principles Studies: Recent Progress and Remaining Challenges. *Ind. Eng. Chem. Res.* **2017**, *56* (24), 6887-6899. DOI: 10.1021/acs.iecr.7b00213.
(101) Yang, X.; Rees, R. J.; Conway, W.; Puxty, G.; Yang, Q.; Winkler, D. A. Computational Modeling and Simulation of CO2 Capture by Aqueous Amines. *Chemical Reviews* **2017**, *117* (14), 9524-9593. DOI: 10.1021/acs.chemrev.6b00662.
(102) Tian, Z.; Dai, S.; Jiang, D.-e. What can molecular simulation do for global warming? *WIREs Computational Molecular Science* **2016**, *6* (2), 173-197, https://doi.org/10.1002/wcms.1241. DOI: https://doi.org/10.1002/wcms.1241 (acccessed 2020/12/12).
(103) da Silva, E. F.; Svendsen, H. F. Ab Initio Study of the Reaction of Carbamate Formation from CO2 and Alkanolamines. *Ind. Eng. Chem. Res.* **2004**, *43* (13), 3413-3418. DOI: 10.1021/ie030619k.
(104) Shim, J.-G.; Kim, J.-H.; Jhon, Y. H.; Kim, J.; Cho, K.-H. DFT Calculations on the Role of Base in the Reaction between CO2 and Monoethanolamine. *Ind. Eng. Chem. Res.* **2009**, *48* (4), 2172-2178. DOI: 10.1021/ie800684a.
(105) da Silva, E. F.; Svendsen, H. F. Computational chemistry study of reactions, equilibrium and kinetics of chemical CO2 absorption. *International Journal of Greenhouse Gas Control* **2007**, *1* (2), 151-157. DOI: https://doi.org/10.1016/S1750-5836(07)00022-9.
(106) Arstad, B.; Blom, R.; Swang, O. CO2 Absorption in Aqueous Solutions of Alkanolamines: Mechanistic Insight from Quantum Chemical Calculations. *The Journal of Physical Chemistry A* **2007**, *111* (7), 1222-1228. DOI: 10.1021/jp065301v.
(107) Sumon, K. Z.; Bains, C. H.; Markewich, D. J.; Henni, A.; East, A. L. L. Semicontinuum Solvation Modeling Improves Predictions of Carbamate Stability in the CO2 + Aqueous Amine Reaction. *The Journal of Physical Chemistry B* **2015**, *119* (37), 12256-12264. DOI: 10.1021/acs.jpcb.5b06076.
(108) Xie, H.-B.; Zhou, Y.; Zhang, Y.; Johnson, J. K. Reaction Mechanism of Monoethanolamine with CO2 in Aqueous Solution from Molecular Modeling. *The Journal of Physical Chemistry A* **2010**, *114* (43), 11844-11852. DOI: 10.1021/jp107516k.
(109) Hwang, G. S.; Stowe, H. M.; Paek, E.; Manogaran, D. Reaction mechanisms of aqueous monoethanolamine with carbon dioxide: a combined quantum chemical and molecular dynamics study. *Phys. Chem. Chem. Phys.* **2015**, *17* (2), 831-839, 10.1039/C4CP04518A. DOI: 10.1039/C4CP04518A.

(110) Guido, C. A.; Pietrucci, F.; Gallet, G. A.; Andreoni, W. The Fate of a Zwitterion in Water from ab Initio Molecular Dynamics: Monoethanolamine (MEA)-CO2. *J. Chem. Theory Comput.* **2013**, *9* (1), 28-32. DOI: 10.1021/ct301071b.
(111) Han, B.; Zhou, C.; Wu, J.; Tempel, D. J.; Cheng, H. Understanding CO2 Capture Mechanisms in Aqueous Monoethanolamine via First Principles Simulations. *The Journal of Physical Chemistry Letters* **2011**, *2* (6), 522-526. DOI: 10.1021/jz200037s.
(112) Sumon, K. Z.; Henni, A.; East, A. L. L. Molecular Dynamics Simulations of Proposed Intermediates in the CO2 + Aqueous Amine Reaction. *The Journal of Physical Chemistry Letters* **2014**, *5* (7), 1151-1156. DOI: 10.1021/jz500237v.
(113) Ma, C.; Pietrucci, F.; Andreoni, W. Capture and Release of CO2 in Monoethanolamine Aqueous Solutions: New Insights from First-Principles Reaction Dynamics. *J. Chem. Theory Comput.* **2015**, *11* (7), 3189-3198. DOI: 10.1021/acs.jctc.5b00379.
(114) Ma, C.; Pietrucci, F.; Andreoni, W. Capturing CO2 in Monoethanolamine (MEA) Aqueous Solutions: Fingerprints of Carbamate Formation Assessed with First-Principles Simulations. *The Journal of Physical Chemistry Letters* **2014**, *5* (10), 1672-1677. DOI: 10.1021/jz5006253.
(115) Matsuzaki, Y.; Yamada, H.; Chowdhury, F. A.; Higashii, T.; Onoda, M. Ab Initio Study of CO2 Capture Mechanisms in Aqueous Monoethanolamine: Reaction Pathways for the Direct Interconversion of Carbamate and Bicarbonate. *The Journal of Physical Chemistry A* **2013**, *117* (38), 9274-9281. DOI: 10.1021/jp406636a.
(116) Orestes, E.; Machado Ronconi, C.; Carneiro, J. W. d. M. Insights into the interactions of CO2 with amines: a DFT benchmark study. *Phys. Chem. Chem. Phys.* **2014**, *16* (32), 17213-17219, 10.1039/C4CP02254H. DOI: 10.1039/C4CP02254H.
(117) Mindrup, E. M.; Schneider, W. F. Computational Comparison of the Reactions of Substituted Amines with CO2. *ChemSusChem* **2010**, *3* (8), 931-938. DOI: https://doi.org/10.1002/cssc.201000060.
(118) Gangarapu, S.; Wierda, G. J.; Marcelis, A. T. M.; Zuilhof, H. Quantum Chemical Studies on Solvents for Post-Combustion Carbon Dioxide Capture: Calculation of pKa and Carbamate Stability of Disubstituted Piperazines. *ChemPhysChem* **2014**, *15* (9), 1880-1886. DOI: https://doi.org/10.1002/cphc.201301217.
(119) Gangarapu, S.; Marcelis, A. T. M.; Zuilhof, H. Improving the Capture of CO2 by Substituted Monoethanolamines: Electronic Effects of Fluorine and Methyl Substituents. *ChemPhysChem* **2012**, *13* (17), 3973-3980, https://doi.org/10.1002/cphc.201200471. DOI: https://doi.org/10.1002/cphc.201200471 (acccessed 2020/12/12).
(120) Jhon, Y. H.; Shim, J.-G.; Kim, J.-H.; Lee, J. H.; Jang, K.-R.; Kim, J. Nucleophilicity and Accessibility Calculations of Alkanolamines: Applications to Carbon Dioxide Absorption Reactions. *The Journal of Physical Chemistry A* **2010**, *114* (49), 12907-12913. DOI: 10.1021/jp105914c.
(121) Li, H.-C.; Chai, J.-D.; Tsai, M.-K. Assessment of dispersion-improved exchange-correlation functionals for the simulation of CO2 binding by alcoholamines. *Int. J. Quantum Chem.* **2014**, *114* (12), 805-812. DOI: https://doi.org/10.1002/qua.24670.
(122) Barlow, J. M. C., Lauren; Zhang, Zisheng; Bim, Daniel; Ripley, Katelyn; Zito, Alessandra; Brushett, Fikile; Alexandrova, Anastassia; Yang, Jenny Y. Molecular Design of Redox Carriers for Electrochemical CO2 Capture and Concentration. *Chem. Soc. Rev.* **2022**, *accepted*.
(123) Bell, W. L. M., A.; Smart, J. C.; DuBois, D. L. . Synthesis and Evaluation of CO2 Carriers. *SAE Technical Papers* **1988**, 881078. DOI: 10.4271/881078.
(124) DuBois, D. L.; Miedaner, A.; Bell, W.; Smart, J. C. Chapter 4 - Electrochemical Concentration of Carbon Dioxide. In *Electrochemical and Electrocatalytic Reactions of Carbon Dioxide*, Sullivan, B. P. Ed.; Elsevier, 1993; pp 94-117.

(125) Scovazzo, P.; Poshusta, J.; DuBois, D.; Koval, C.; Noble, R. Electrochemical Separation and Concentration of <1% Carbon Dioxide from Nitrogen. *J. Electrochem. Soc.* **2003**, *150* (5), D91-D98. DOI: 10.1149/1.1566962.
(126) Clarke, L. E.; Leonard, M. E.; Hatton, T. A.; Brushett, F. R. Thermodynamic Modeling of CO2 Separation Systems with Soluble, Redox-Active Capture Species. *Ind. Eng. Chem. Res.* **2022**, *61* (29), 10531-10546. DOI: 10.1021/acs.iecr.1c04185.
(127) Mizen, M. B.; Wrighton, M. S. Reductive Addition of CO 2 to 9,10-Phenanthrenequinone. *J. Electrochem. Soc.* **1989**, *136* (4), 941-946. DOI: 10.1149/1.2096891.
(128) Nagaoka, T.; Nishii, N.; Fujii, K.; Ogura, K. Mechanisms of reductive addition of CO2 to quinones in acetonitrile. *J. Electroanal. Chem.* **1992**, *322* (1), 383-389. DOI: https://doi.org/10.1016/0022-0728(92)80090-Q.
(129) Qiao, X.; Li, D.; Cheng, L.; Jin, B. Mechanism of electrochemical capture of CO2 via redox cycle of chlorinated 1,4-naphthoquinone in BMIMBF4: An in-situ FT-IR spectroelectrochemical approach. *J. Electroanal. Chem.* **2019**, *845*, 126-136. DOI: https://doi.org/10.1016/j.jelechem.2019.05.057.
(130) Scovazzo, P.; Poshusta, J.; DuBois, D.; Koval, C.; Noble, R. Electrochemical Separation and Concentration of <1% Carbon Dioxide from Nitrogen. *J. Electrochem. Soc.* **2003**, *150* (5), D91. DOI: 10.1149/1.1566962.
(131) Schmidt, M. H.; Miskelly, G. M.; Lewis, N. S. Effects of Redox Potential, Steric Configuration, Solvent, and Alkali Metal Cations on the Binding of Carbon Dioxide to Cobalt(I) and Nickel(I) Macrocycles. *J. Am. Chem. Soc.* **1990**, *112* (9), 3420-3426. DOI: 10.1021/ja00165a027.
(132) Appel, A. M.; Newell, R.; DuBois, D. L.; Rakowski DuBois, M. Concentration of Carbon Dioxide by Electrochemically Modulated Complexation with a Binuclear Copper Complex. *Inorg. Chem.* **2005**, *44* (9), 3046-3056. DOI: 10.1021/ic050023k.
(133) Hitoshi, I.; Tomoyuki, O.; Tomohiro, Y.; Katsutoshi, O. Interaction between CO2 and Electrochemically Reduced Species of N-propyl-4,4'-bipyridinium Cation. *Chem. Lett.* **1994**, *23* (5), 905-908. DOI: 10.1246/cl.1994.905.
(134) Singh, P.; Tarakeshwar, P.; Buttry, D. A. Experimental, Simulation, and Computational Study of the Interaction of Reduced Forms of N-Methyl-4,4'-Bipyridinium with CO2. *ChemElectroChem* **2020**, *7* (2), 469-475. DOI: 10.1002/celc.201901884.
(135) Ranjan, R.; Olson, J.; Singh, P.; Lorance, E. D.; Buttry, D. A.; Gould, I. R. Reversible Electrochemical Trapping of Carbon Dioxide Using 4,4'-Bipyridine That Does Not Require Thermal Activation. *Journal of Physical Chemistry Letters* **2015**, *6* (24), 4943-4946. DOI: 10.1021/acs.jpclett.5b02220.
(136) Singh, P.; Rheinhardt, J. H.; Olson, J. Z.; Tarakeshwar, P.; Mujica, V.; Buttry, D. A. Electrochemical Capture and Release of Carbon Dioxide Using a Disulfide–Thiocarbonate Redox Cycle. *J. Am. Chem. Soc.* **2017**, *139* (3), 1033-1036. DOI: 10.1021/jacs.6b10806.
(137) Bell, W. L.; Miedaner, A.; Smart, J. C.; DuBois, D. L.; Verostko, C. E. Synthesis and Evaluation of Electroactive CO_2 Carriers. *SAE Transactions* **1988**, *97*, 544-552. (acccessed 2020/04/04/).JSTOR.
(138) Namazian, M.; Zare, H. R.; Yousofian-Varzaneh, H. Electrochemical behavior of tetrafluoro-p-benzoquinone at the presence of carbon dioxide: Experimental and theoretical studies. *Electrochim. Acta* **2016**, *196*, 692-698. DOI: https://doi.org/10.1016/j.electacta.2016.02.159.
(139) Zito, A. M.; Bím, D.; Vargas, S.; Alexandrova, A. N.; Yang, J. Y. Computational and Experimental Design of Quinones for Electrochemical CO2 Capture and Concentration. *ACS Sustainable Chemistry & Engineering* **2022**, *10* (34), 11387-11395. DOI: 10.1021/acssuschemeng.2c03463.
(140) Comeau Simpson, T.; Durand, R. R. Reactivity of carbon dioxide with quinones. *Electrochim. Acta* **1990**, *35* (9), 1399-1403. DOI: https://doi.org/10.1016/0013-4686(90)85012-C.
(141) Schimanofsky, C.; Wielend, D.; Kröll, S.; Lerch, S.; Werner, D.; Gallmetzer, J. M.; Mayr, F.; Neugebauer, H.; Irimia-Vladu, M.; Portenkirchner, E.; et al. Direct Electrochemical CO2 Capture Using

Substituted Anthraquinones in Homogeneous Solutions: A Joint Experimental and Theoretical Study. *The Journal of Physical Chemistry C* **2022**, *126* (33), 14138-14154. DOI: 10.1021/acs.jpcc.2c03129.
(142) Gupta, N.; Linschitz, H. Hydrogen-Bonding and Protonation Effects in Electrochemistry of Quinones in Aprotic Solvents. *J. Am. Chem. Soc.* **1997**, *119* (27), 6384-6391. DOI: 10.1021/ja970028j.
(143) De Sousa Bulhõesw, L. O.; Zara, A. J. The effect of carbon dioxide on the electroreduction of 1,4-benzoquinone. *Journal of Electroanalytical Chemistry and Interfacial Electrochemistry* **1988**, *248* (1), 159-165. DOI: https://doi.org/10.1016/0022-0728(88)85158-1.
(144) Aranzaes, J. R.; Daniel, M.-C.; Astruc, D. Metallocenes as references for the determination of redox potentials by cyclic voltammetry — Permethylated iron and cobalt sandwich complexes, inhibition by polyamine dendrimers, and the role of hydroxy-containing ferrocenes. *Can. J. Chem.* **2006**, *84* (2), 288-299. DOI: 10.1139/v05-262.
(145) Zanello, P. *Inorganic Electrochemistry: Theory, Practice and Application*; 2003.
(146) Fan, H.; Cheng, L.; Jin, B. Investigation on electrochemical capture of CO2 in p-Benzoquinone solutions by in situ FT-IR spectroelectrochemistry. *Electrochim. Acta* **2019**, *324*, 134882. DOI: https://doi.org/10.1016/j.electacta.2019.134882.
(147) Voskian, S.; Hatton, T. A. Faradaic electro-swing reactive adsorption for CO2 capture. *Energy & Environmental Science* **2019**, *12* (12), 3530-3547. DOI: 10.1039/C9EE02412C.
(148) Liu, Y.; Ye, H.-Z.; Diederichsen, K. M.; Van Voorhis, T.; Hatton, T. A. Electrochemically mediated carbon dioxide separation with quinone chemistry in salt-concentrated aqueous media. *Nature Communications* **2020**, *11* (1), 2278. DOI: 10.1038/s41467-020-16150-7.
(149) Nagaoka, T.; Okazaki, S.; Fujinaga, T. Ion-pair effects on the electroreduction of carbonyl compounds in N,-Dimethylformamide. *Journal of Electroanalytical Chemistry and Interfacial Electrochemistry* **1982**, *133* (1), 89-99. DOI: https://doi.org/10.1016/0022-0728(82)87008-3.
(150) Kim, Y.-R.; Kim, R. S.; Kang, S. K.; Choi, M. G.; Kim, H. Y.; Cho, D.; Lee, J. Y.; Chang, S.-K.; Chung, T. D. Modulation of Quinone PCET Reaction by Ca2+ Ion Captured by Calix[4]quinone in Water. *J. Am. Chem. Soc.* **2013**, *135* (50), 18957-18967. DOI: 10.1021/ja410406e.
(151) Peover, M. E.; Davies, J. D. The influence of ion-association on the polarography of quinones in dimethylformamide. *Journal of Electroanalytical Chemistry (1959)* **1963**, *6* (1), 46-53. DOI: https://doi.org/10.1016/0022-0728(63)80116-3.
(152) Aimoto, Y.; Koshiba, K.; Yamauchi, K.; Sakai, K. A family of molecular nickel hydrogen evolution catalysts providing tunable overpotentials using ligand-centered proton-coupled electron transfer paths. *Chemical Communications* **2018**, *54* (91), 12820-12823, 10.1039/C8CC07467D. DOI: 10.1039/C8CC07467D.
(153) Delgado, M.; Wolf, R. E.; Hartman, J. R.; McCafferty, G.; Yagbasan, R.; Rawle, S. C.; Watkin, D. J.; Cooper, S. R. Redox-active crown ethers. Electrochemical and electron paramagnetic resonance studies on alkali metal complexes of quinone crown ethers. *J. Am. Chem. Soc.* **1992**, *114* (23), 8983-8991. DOI: 10.1021/ja00049a032.
(154) Eggins, B. R. Interpretation of electrochemical reduction and oxidation waves of quinone–hydroquinone system in acetonitrile. *Journal of the Chemical Society D: Chemical Communications* **1969**, (21), 1267-1268, 10.1039/C29690001267. DOI: 10.1039/C29690001267.
(155) Barlow, J. M.; Yang, J. Y. Oxygen-Stable Electrochemical CO2 Capture and Concentration with Quinones Using Alcohol Additives. *J. Am. Chem. Soc.* **2022**, *144* (31), 14161-14169. DOI: 10.1021/jacs.2c04044.
(156) Kajiwara, T.; Yamaguchi, T.; Kido, H.; Kawabata, S.; Kuroda, R.; Ito, T. A dinucleating bis(dimethylcyclam) ligand and its dinickel(II) and dizinc(II) complexes with the face-to-face ring arrangement. *Inorg. Chem.* **1993**, *32* (23), 4990-4991. DOI: 10.1021/ic00075a003.
(157) Murase, I.; Vuckovic, G.; Kodera, M.; Harada, H.; Matsumoto, N.; Kida, S. Synthesis and characterization of copper(II), nickel(II), and cobalt(II) binuclear complexes with a new tricyclic

octadentate ligand, 1,5,8,12,15,19,22,26-octaazatricyclo[17.9.2.25,15]dotriacontane (tcoa): trapping of carbon dioxide in a neutral aqueous solution. *Inorg. Chem.* **1991**, *30* (4), 728-733. DOI: 10.1021/ic00004a024.
(158) Harada, H.; Kodera, M.; Vuckovic, G.; Matsumoto, N.; Kida, S. Preparation and redox chemistry of novel carbonato-bridged cobalt(II) complexes with 1,4,8,11-tetrakis(2-aminoethyl)-1,4,8,11-tetraazacyclotetradecane and 1,4,8,11-tetrakis(pyridylmethyl)-1,4,8,11-tetraazacyclotetradecane. *Inorg. Chem.* **1991**, *30* (6), 1190-1194. DOI: 10.1021/ic00006a007.
(159) Newell, R.; Appel, A.; DuBois, D. L.; Rakowski DuBois, M. Studies of Bicarbonate Binding by Dinuclear and Mononuclear Ni(II) Complexes. *Inorg. Chem.* **2005**, *44* (2), 365-373. DOI: 10.1021/ic049202c.
(160) Ranjan, R.; Olson, J.; Singh, P.; Lorance, E. D.; Buttry, D. A.; Gould, I. R. Reversible Electrochemical Trapping of Carbon Dioxide Using 4,4'-Bipyridine That Does Not Require Thermal Activation. *The Journal of Physical Chemistry Letters* **2015**, *6* (24), 4943-4946. DOI: 10.1021/acs.jpclett.5b02220.
(161) Stueber, D.; Orendt, A. M.; Facelli, J. C.; Parry, R. W.; Grant, D. M. Carbonates, Thiocarbonates, and the Corresponding Monoalkyl Derivatives: III. The 13C Chemical Shift Tensors in Potassium Carbonate, Bicarbonate and Related Monomethyl Derivatives. *Solid State Nucl. Magn. Reson.* **2002**, *22* (1), 29-49. DOI: https://doi.org/10.1006/snmr.2002.0061.
(162) Stueber, D.; Arif, A. M.; Grant, D. M.; Parry, R. W. Carbonates, Thiocarbonates, and the Corresponding Monoalkyl Derivatives. 2. X-ray Crystal Structure of Potassium Methyltrithiocarbonate (KS2CSCH3). *Inorg. Chem.* **2001**, *40* (8), 1912-1914. DOI: 10.1021/ic001227y.
(163) Harris, D.; Bushnell, E. Density Functional Theory Study of the Capture and Release of Carbon Dioxide by Benzyl–Disulfide, −Diselenide, and −Ditelluride. *The Journal of Physical Chemistry A* **2019**, *123* (15), 3383-3388. DOI: 10.1021/acs.jpca.9b01862.
(164) Gangi, D. A.; Durand, R. R. Binding of carbon dioxide to cobalt and nickel tetra-aza macrocycles. *J. Chem. Soc., Chem. Commun.* **1986**, (9), 697-699, 10.1039/C39860000697. DOI: 10.1039/C39860000697.
(165) Bard, A. J.; Faulkner, L. R. *Electrochemical Methods: Fundamentals and Application*; John Wiley & Sons, Inc., 2001.
(166) Creutz, C.; Schwarz, H. A.; Wishart, J. F.; Fujita, E.; Sutin, N. Thermodynamics and kinetics of carbon dioxide binding to two stereoisomers of a cobalt(I) macrocycle in aqueous solution. *J. Am. Chem. Soc.* **1991**, *113* (9), 3361-3371. DOI: 10.1021/ja00009a022.
(167) Creutz, C. Chapter 2 - Carbon Dioxide Binding to Transition-Metal Centers. In *Electrochemical and Electrocatalytic Reactions of Carbon Dioxide*, Sullivan, B. P. Ed.; Elsevier, 1993; pp 19-67.
(168) Benesi, H. A.; Hildebrand, J. H. A Spectrophotometric Investigation of the Interaction of Iodine with Aromatic Hydrocarbons. *J. Am. Chem. Soc.* **1949**, *71* (8), 2703-2707. DOI: 10.1021/ja01176a030.